BAE 655-Wireless Communications

1.1 Structure of a Digital Communication System

The overall focus here is on the structure of a digital communication system operating over a wireless channel. We will consider *conventional* systems, using a single antenna at the transmitter and, possibly, *diversity reception*, and MIMO systems. One of the most powerful techniques available to improve the performance and throughput of wireless transmission is that of *diversity*. In fact, diversity creates multiple copies of the transmitted signal at the receiver. In principle, these copies are uncorrelated, so that when one copy is deeply faded due to the wireless channel, the others are not. This allows for significant improvement in both the error performance and throughput of wireless transmission systems. The concept of diversity in receivers has been known for many years [13]; however, in recent years there has been much work in developing techniques to achieve diversity at the transmitter [14, 15] and to combine transmit and receive diversity through the use of *space-time coding* [16].

Systems that combine transmit and receive diversity are known as MIMO systems, which may in a sense be considered as the most general system architecture. Such systems include space-time coded systems [16] and the so-called *Bell Labs Layered Space-Time* (BLAST) [17] or *spatial multiplexing* architectures. The latter have been shown to allow for major increases in the available channel capacity [18] and a consequent increase in the efficiency of use of the available radio spectrum. Note that capacity provides a theoretical upper limit on the throughput that can be achieved in a given channel.

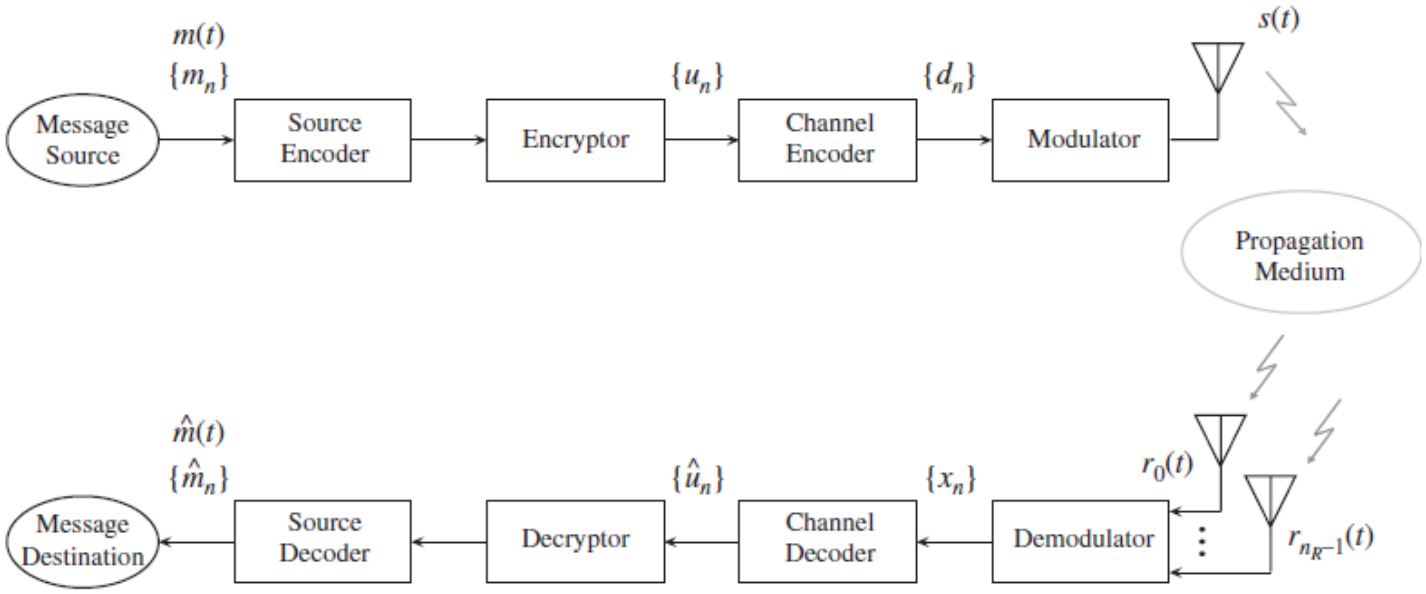

Figure 1.1 Block diagram of a conventional digital communication system with *diversity reception*.

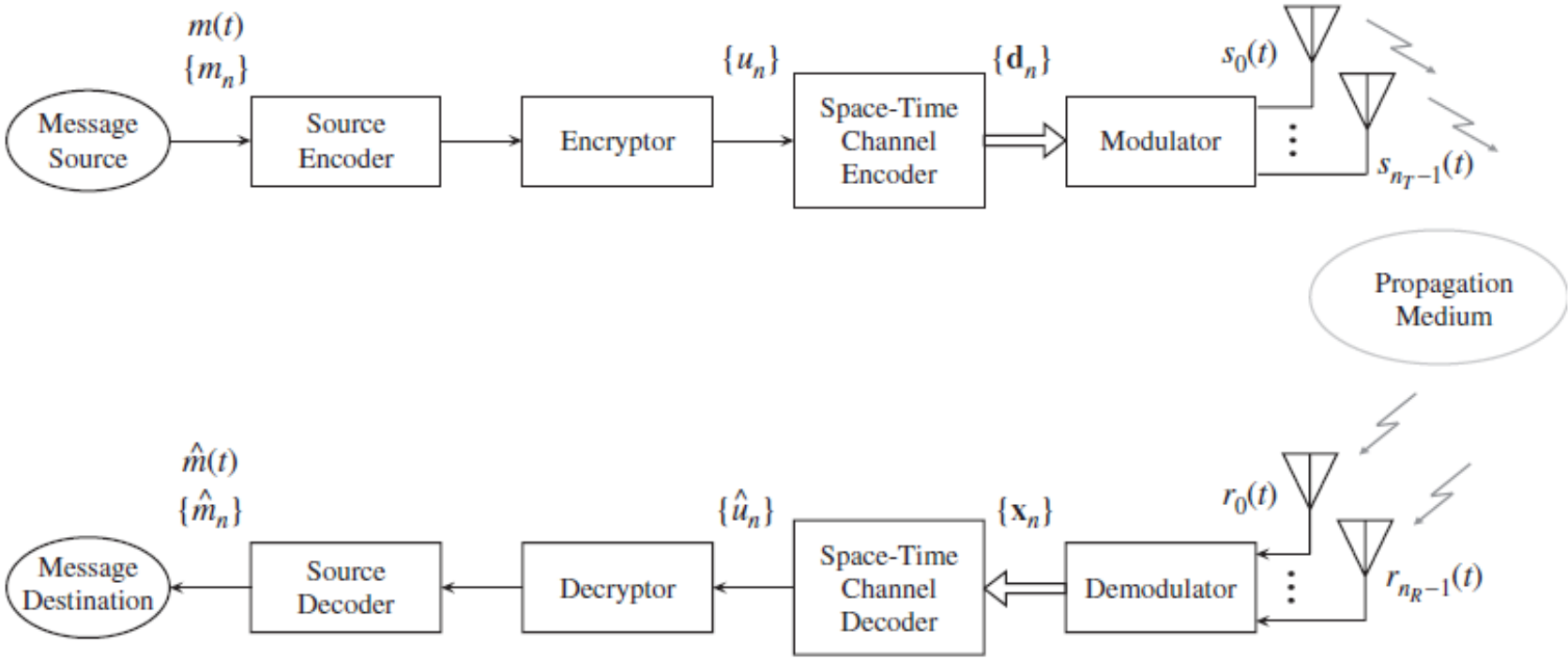

Figure 1.2 Block diagram of a *space-time* digital communication system.

A wireless communication system designer does not usually have complete control over the *communication channel*. With reference to Figures 1.1 and 1.2, this includes the *propagation medium* (i.e., the physical space through which the electromagnetic signal radiated by the transmit antenna travels), the final section of the transmitter (e.g., the transmit antenna and filtering/amplification stages preceding it), and the initial section of the receiver (e.g., the receive antenna and low noise amplifier

Any communication channel also adds *random noise*, which is generated by both external sources
(e.g., cosmic and atmospheric signals, and interference) and by the electronic devices in the receiver

- The *source encoder* processes the source message stream to remove its natural *redundancies*. This can result in appreciable reduction of the bit rate, sometimes achieved, however, at the price of an information loss. Despite this, the original message stream can be recovered by the source decoder at the receiver within some *specified fidelity*.
- The *encryptor*, if present, adds security coding to the data sequence generated by the source encoder. This result is achieved by a coding algorithm turning the unciphered data (usually called *plaintext*) into a new discrete sequence $\{u_n\}$ (called *ciphertext*). The encryption algorithm involves a parameter, called the *key*, knowledge of which at the receiver is essential to deciphering. One class of modern and well-known ciphering techniques, known as *public-key encryption*, relies on a double key mechanism, that is, on the use of a *public key* (potentially known to anyone) for enciphering and on a *private key* (known, in principle, only to the message destination) for deciphering [20].
- The *channel encoder* introduces an error-correction capability, so that most (possibly all) of the errors due to channel noise and distortion can be removed or corrected at the receiver. To achieve this target, the channel encoder introduces *memory* and *redundancy* into the coded sequence. The presence of redundancy is seen from the fact that, in a given time interval, the number of bits generated by the channel encoder is larger than the number of the information bits processed by it. Memory can be related to the fact that, generally speaking, each bit feeding the encoder influences multiple bits at its output. As discussed in Part II of this book, the receiver exploits both these properties to improve the reliability of its decisions.
- The *modulator* is fed by the symbol sequence $\{d_n\}$ (each symbol belongs to a multilevel alphabet) and generates an analog signal $s(t)$, which consists of the concatenation of waveforms belonging to some *finite alphabet of signals*. In practice, this device represents the interface between the stream of discrete data and the real communication medium. Therefore, it accomplishes multiple tasks (including frequency up-conversion) and power amplification and can incorporate transducers (e.g., multiple transmit antennas).

In general, the receiver has $n_R \geq 1$ antennas. The lth antenna (with $l = 0, 1, \ldots, n_R - 1$) feeds the *demodulator* with the noisy *radio-frequency* (RF) signal:

$$r_l(t) = z_l(t) + n_l(t), \tag{1.1}$$

where $z_l(t)$ and $n_l(t)$ represent the *useful signal component* (i.e., the response to $s(t)$ of the communication channel including the transmitter and the transmit/receive antennas in the absence of noise) and the *random noise* at the receive antenna terminals, respectively. The demodulator processes the waveforms $\{r_l(t)\}$ of (1.1), to extract a set of *synchronization parameters* (such as the phase and frequency of the carrier associated with $z_l(t)$, and timing information), and in many cases an *estimate* of the communication channel response. Then it uses this information to perform signal

The *channel decoder* exploits the information provided by the demodulator, to try to find the *most likely* data sequence $\{\hat{u}_n\}$ that has generated the coded sequence $\{d_n\}$. Note that the availability of soft information allows the decoder to improve the quality of its decisions with respect to the case of knowledge of hard information.

The task accomplished by the *decryptor* is the inverse to that of the encryptor. This task can be carried out successfully if both the ciphering algorithm and its key are known.

The *source decoder* processes an estimate of the binary data generated by the source encoder to generate a message in a proper format (the data sequence $\{\hat{m}_n\}$ or the analog signal $\hat{m}(t)$ in Figure 1.1) for the destination.

Finally, we note that the system of Figure 1.1 is characterized by a communication channel with a *single* input (corresponding to a single transmit antenna) and *multiple* outputs, to be processed by a receiver equipped with $n_R \geq 1$ antennas. For this reason, the communication system can be classified as SIMO. In particular, if $n_R = 1$, we have a SISO system.

The scheme illustrated in Figure 1.2 generalizes that of Figure 1.1, since it represents a system with $n_T > 1$ transmit antennas, resulting in a MIMO system. In such a system, the channel encoder, in response to the discrete data sequence $\{u_n\}$, generates a sequence of *vectors* $\{\mathbf{d}_n\}$, each consisting of n_T different elements. For any n, the kth element $d_n[k]$ (with $k = 0, 1, \ldots, n_T - 1$) of $\mathbf{d}_n$ is transmitted by the modulator as the RF signal $s_k(t)$ radiated by the kth antenna. Therefore, the redundancy and memory introduced by the encoder are spread over both *time* (as in the SIMO scenario described above) and *space* using *distinct transmit antennas* (*transmit diversity*). This is commonly referred to as *space-time* (ST) channel coding [16]. Generally speaking, each receive antenna observes a linear combination of all n_T transmitted signals. In fact, the noisy signal captured by the lth receive antenna can be expressed as:

$$r_l(t) = \sum_{k=0}^{n_T-1} z_{kl}(t) + n_l(t), \tag{1.2}$$

with $l = 0, 1, \ldots, n_R - 1$, where $z_{kl}(t)$ and $n_l(t)$ respectively represent the useful signal component

Technically important results in the development of systems equipped with antenna arrays have also been obtained using the transmission technique known as MIMO-OFDM.[3] In this case spatial multiplexing is combined with *frequency division multiplexing* (FDM), so that spatial diversity is jointly exploited with spectral or frequency diversity. The last form of diversity arises due to the fact that, in a multipath channel, distinct spectral components of the transmitted signal undergo different phase/amplitude changes. Again in the development of MIMO-OFDM systems the derivation of many of theoretical results has been followed by the development of prototypes (e.g., see [24, 25, 26]) and, later, by the implementation of ASICs for modern wireless communications systems (e.g., in local area radio networks).

2 Wireless Channels

2.1 Introduction

In wireless communication systems the channel introduces *random variations with time and/or frequency in both the amplitude and phase of the transmitted signal*. These phenomena are collectively known as *fading and dispersion* [19, 44–46]. The study of fading, dispersive channels is the main subject of this chapter.

Fading originates due to various causes. The most common is the presence of *multiple propagation paths*, that is, the existence of a number of paths along which an electromagnetic signal propagates from a transmitting antenna to the receiving one [19, 47, 48]. The presence of these multiple paths is normally due to *reflection*, *diffraction* and *scattering* caused by objects in the propagation medium

When a communication system operates over a *time-dispersive* channel (a channel affected by multiple propagation paths), the distinct *echoes* of the transmitted signal captured by a receive antenna have different amplitudes and phases. These differences in general depend on *both frequency and time* and, if we neglect noise, the received signal consists of the linear combination of multiple echoes or replicas of the transmitted signal modified, in spectral content, according to the time variability of the medium.

Time variability manifests itself as *time selectivity* in the form of fluctuations in the intensity of the received signal. This variability is usually due to relative motion between receiver and transmitter and/or to environmental changes, producing changes in the characteristics of the various propagation paths. To mathematically describe channel behavior over a realistic time scale, channel models char-

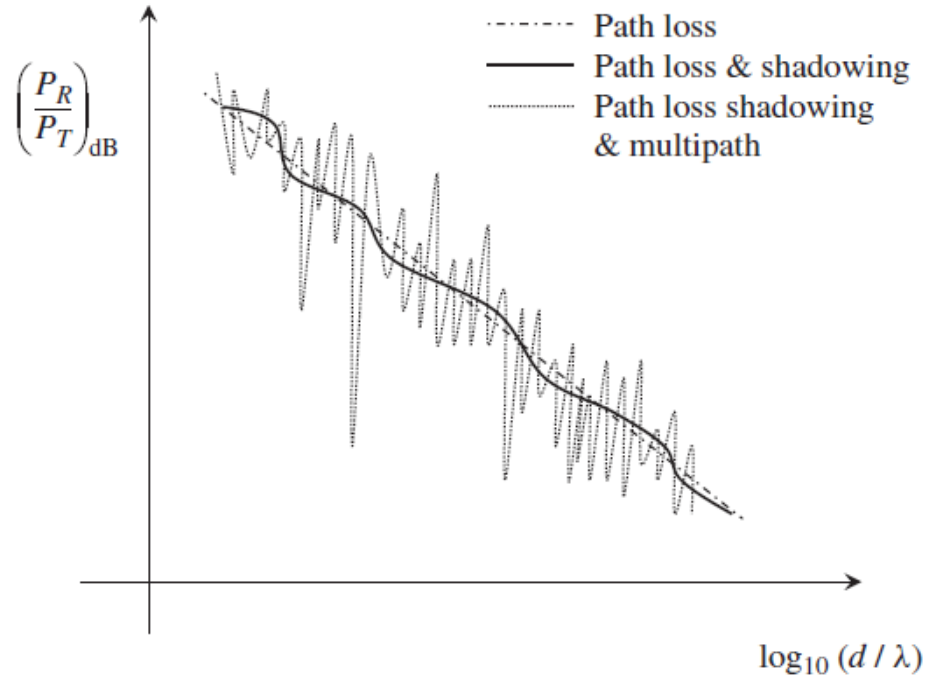

Figure 2.1 Typical behavior (dotted curve) of the ratio, expressed in decibels, between the received power P_R and the transmitted power P_T versus the transmitter–receiver distance d (normalized to the link wavelength λ) in a wireless communication system operating over a fading channel. The contributions due to path loss (dot-dashed curve) and to the joint effect of this loss and shadowing (continuous line) are also shown.

$\bar{P}_R(d)$ in the *far field region*, for a given transmitted power P_T and at a transmitter–receiver distance d, can be assessed by evaluating the *average path loss* (or *propagation loss*) as:

$$L(d) \triangleq \frac{P_T}{\bar{P}_R(d)} \tag{2.1}$$

or, in decibels, as:

$$L(d)_{\text{dB}} \triangleq 10 \log_{10} L(d) = L(d_0)_{\text{dB}} + 10\, n \log_{10} \left(\frac{d}{d_0} \right), \tag{2.2}$$

where the parameters d_0 and n are the so-called *close-in reference distance* and *path loss exponent*, respectively. This does not include the random effects of shadowing, which can be accounted for by adding a random term X to the *right-hand side* (RHS) of (2.2), so that the total power loss in decibels is given by:

$$L_t(d)_{\text{dB}} = L(d)_{\text{dB}} + X. \tag{2.3}$$

past, the interest in new *personal communication systems* (PCSs) [59] has also fostered research on electromagnetic propagation in *urban microcells*, each consisting of a small area, with a radius of a few hundred meters. These exhibit channel properties that are substantially different than those of macrocells. This is due to the fact that BS antennas in microcells are placed below the roof line of surrounding buildings (typically at a height of 3–10 m) and BS powers are lower (0.1–1 W). For these reasons, the cell is shaped by the buildings themselves and electromagnetic waves propagate along shorter paths [56].

Indoor channel models are of interest, for instance, in the study of *cordless* telephony and WLANs operating in buildings devoted to different uses (offices, depots, stores, etc.) [60–63]. In the literature dealing with the radio coverage inside buildings, two distinct situations are considered. In the first, the transmitter is placed on the roof of a building different from that in which the receiver is operating, whereas in the second the transmitter and receiver are placed in the same building. In

Table 2.1 Typical values of the *path loss exponent n* in various environments

Environment	Range of n
Free space	2
Urban macrocells	3.7–6.5
Urban microcells	2.7–3.5
Office in a building (same floor)	1.6–3.5
Office in a building (different floors)	2–6
Warehouse	1.8–2.2
Factory	1.6–3.3
House	3

2.2.1 *Input–Output Characterization of a SISO Wireless Channel*

2.2.1.1 General Case

The input–output behavior of any LTVS is fully described by its *time-variant impulse response* (TVIR), defined as the system response to an impulse or *Dirac delta function* delayed by τ sec. More specifically, the TVIR is defined as:

$$g(t, t-\tau) = \Upsilon_{RF}[\delta(t-\tau)], \tag{2.5}$$

where t represents *time*, τ represents *delay* (with respect to the reference instance $t = 0$) in the application of the impulse to the system, and the operator $\Upsilon_{RF}[\cdot]$ describes the transformation accomplished by the LTVS. Note that the *dependence of the system physical behavior on time* is explicitly indicated by the presence of t as the first variable in the argument of the TVIR. The dependence of

the TVIR on the delay variable, τ, accounts for the *time dispersion* introduced by the channel, that is, for the generation of the multiple echoes of the transmitted signal.

In our analysis the channel is fed by a *real* RF signal $x_{RF}(t)$, having a central frequency f_c, and results in the *real* RF response:

$$y_{RF}(t) = \Upsilon_{RF}[x_{RF}(t)]. \tag{2.6}$$

It is not difficult to show that, given the TVIR of (2.5), $y_{RF}(t)$ in (2.6) can be expressed as [78]:

$$y_{RF}(t) = \int_{-\infty}^{+\infty} x_{RF}(t-\tau)\, g(t,\tau)\, d\tau. \tag{2.7}$$

This lends itself to a simple interpretation. In fact, it means that the input signal is delayed and multiplied by a differential scattering gain $g(t,\tau)\, d\tau$; this complex factor expresses the modulation due to the scatterers introducing a delay in the interval $(\tau,\ \tau + d\tau)$. For this reason, the system function $g(t,\tau)$ is also called *input delay-spread function* [78].

To simplify the study of system functions, it is useful to adopt an equivalent low-pass representation of the communication channel[6] [79]. We then let $x(t)$, $y(t)$ and $h(t, t-\tau)$ denote the *low-pass equivalent signals* (with respect to the reference frequency f_c) of $x_{RF}(t)$, $y_{RF}(t)$ and $g(t, t-\tau)$ respectively, that is, the complex signals such that:

$$x_{RF}(t) = \mathrm{Re}\{x(t) \exp(j2\pi f_c t)\},$$

$$y_{RF}(t) = \mathrm{Re}\{y(t) \exp(j2\pi f_c t)\},$$

and

$$g(t, t-\tau) = 2\mathrm{Re}\{h(t, t-\tau) \exp(j2\pi f_c t)\}, \tag{2.8}$$

and

$$g(t, t-\tau) = 2\mathrm{Re}\{h(t, t-\tau)\exp(j2\pi f_c t)\}, \tag{2.8}$$

where $h(t,\tau)$ is the so-called *channel impulse response* (CIR) or *input delay spread function* (since it is the low-pass equivalent of $g(t,\tau)$ in (2.5)).[7] Then it can be shown that the RF input–output relationship (2.7) is equivalent to:

$$y(t) = \int_{-\infty}^{+\infty} x(t-\tau)\, h(t,\tau)\, d\tau = \int_{-\infty}^{+\infty} x(\tau)\, h(t, t-\tau)\, d\tau, \tag{2.9}$$

relating the low-pass signals $x(t)$, $y(t)$ and $h(t,\tau)$. Note that, as can be easily inferred from (2.9), $h(t, t-\tau)$ can also be defined as the response of the low-pass equivalent channel to the impulsive excitation $\delta(t-\tau)$, that is:

$$h(t, t-\tau) \triangleq \Upsilon_{BB}[\delta(t-\tau)], \tag{2.10}$$

where $\Upsilon_{BB}[\cdot]$ is the low-pass equivalent of the transformation accomplished by the channel, that is, a transformation such that $y(t) = \Upsilon_{BB}[x(t)]$.

To grasp the physical meaning of (2.9), it is useful to approximate the first integral as a sum. This can be done by discretizing the delay space in a uniform fashion and, in particular, generating the sequence $\tau_i \triangleq i\Delta\tau$, where $i \in \mathbb{Z}$ and $\Delta\tau$ is the discretization step. Then (2.9) can be approximated as:

$$y(t) \cong \sum_{i=-\infty}^{+\infty} x(t-\tau_i)\, h(t,\tau_i)\, \Delta\tau = \sum_{i=-\infty}^{+\infty} a_i(t)\, x(t-\tau_i), \tag{2.11}$$

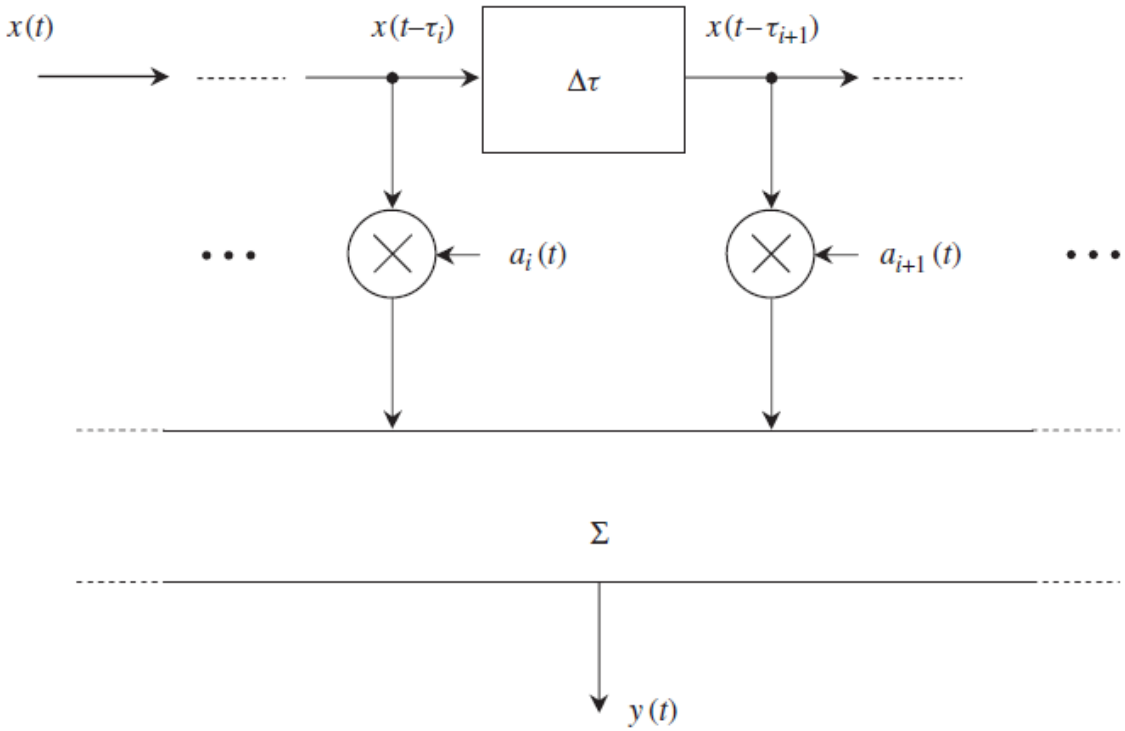

Figure 2.2 Representation of (2.11) (TDL model of a communication channel).

where:

$$a_i(t) \triangleq h(t, \tau_i)\ \Delta\tau. \tag{2.12}$$

where:

$$a_i(t) \triangleq h(t, \tau_i)\ \Delta\tau. \tag{2.12}$$

The input–output relationship of (2.11) is summarized by the block diagram of Figure 2.2, representing the communication channel as a *tapped delay line* (TDL). In Section 2.2.3 we will show that, under certain assumptions, this model provides an *exact* description of a communication channel. In fact, $x(t)$ goes through a *delay line*, consisting of the serial concatenation of an infinite number of identical cells (each introducing a delay of $\Delta\tau$ sec). The ith delayed replica $x(t - \tau_i)$ of $x(t)$ feeds the ith *tap*, accomplishing a multiplication by the complex time-varying gain $a_i(t)$ (2.12). Then the tap outputs are summed, generating an approximation to $y(t)$ (2.9). In other words, the TDL model represents the channel output signal as the superposition of an infinite number of echoes, each having time-varying amplitude and phase.

The CIR is not the only system function that fully describes the input–output behavior of an LTVS. An equivalent description is provided by the so-called *time-variant transfer function* (TVTF) defined as [78]:

$$H(t, f) \triangleq \mathrm{FCT}_{\tau \to f}[h(t, \tau)] = \int_{-\infty}^{+\infty} h(t, \tau)\ \exp(-j2\pi f \tau)\ d\tau, \tag{2.13}$$

where $\mathrm{FCT}_{\tau \to f}[\cdot]$ denotes the *Fourier continuous transform* (FCT) evaluated with respect to the variable τ and leading to an explicit dependence on the *frequency* variable f. From (2.13) the inverse relationship:

$$h(t, \tau) = \mathrm{IFCT}_{f \to \tau}[H(t, f)] = \int_{-\infty}^{+\infty} H(t, f) \exp(j2\pi f \tau)\ df \tag{2.14}$$

is immediately inferred, where IFCT[·] denotes an *inverse Fourier continuous transform* (IFCT). Substituting this in (2.9) produces, after some manipulation:

$$y(t) = \int_{-\infty}^{+\infty} X(f)\ H(t, f)\ \exp(j2\pi f t)\ df, \tag{2.15}$$

which expresses the input–output relationship in a new form, involving $H(t, f)$, and the FCT $X(f)$ of $x(t)$.

Establishing a relationship between the FCT:

$$Y(f) \triangleq \mathrm{FCT}[y(t)] = \int_{-\infty}^{+\infty} y(t) \exp(-j2\pi ft)\, dt \tag{2.16}$$

of the output $y(t)$ of an LTVS and the FCT $X(f)$ of its input signal requires the introduction of a further system function. In fact, substituting (2.15) in the RHS of (2.16) yields, after some manipulation:

$$Y(f) = \int_{-\infty}^{+\infty} X(\alpha)\, \Gamma(f - \alpha, \alpha)\, d\alpha, \tag{2.17}$$

where

$$\Gamma(\nu, f) \triangleq \mathrm{FCT}_{t \to \nu}[H(t, f)] = \int_{-\infty}^{+\infty} H(t, f) \exp(-j2\pi \nu t)\, dt \tag{2.18}$$

is the so-called *output Doppler-spread function* [78]. Note that $\Gamma(\nu, f)$ depends on two spectral variables, namely the frequency f and the *Doppler shift*[8] ν, and that equation (2.17) expresses the

where

$$\Gamma(\nu, f) \triangleq \mathrm{FCT}_{t\to\nu}[H(t, f)] = \int_{-\infty}^{+\infty} H(t, f) \exp(-j2\pi\nu t)\, dt \tag{2.18}$$

is the so-called *output Doppler-spread function* [78]. Note that $\Gamma(\nu, f)$ depends on two spectral variables, namely the frequency f and the *Doppler shift*[8] ν, and that equation (2.17) expresses the output spectrum as a *convolution* between the input spectrum and $\Gamma(\nu, f)$ (2.18). A comparison of (2.17) with (2.9) illustrates a deep structural analogy between these two input–output relationships, referring, however, to different domains. In fact, the latter involves signals defined in the t and τ domains, whereas the former functions are defined in the ν and f domains. This analogy is usually stressed by stating that (2.17) is the *dual* of (2.9) and, in particular, that $\Gamma(\nu, f)$ is the *dual function* of the CIR $h(t, \tau)$ [80]. These considerations are important not only from a mathematical viewpoint, but also from a physical one, since they allow us to understand the real significance of $\Gamma(\nu, f)$. In fact, this function, by duality, could be introduced by evaluating the LTVS response, in the frequency domain, to an *impulsive input spectrum*. In particular, if $X(f) = \delta(f - f_0)$ is selected (corresponding to the time-domain choice $x(t) = \exp(j2\pi f_0 t)$), where f_0 is an arbitrary frequency, then (2.17) produces:

$$Y(f) = \int_{\alpha=-\infty}^{+\infty} \delta(\alpha - f_0)\, \Gamma(f - \alpha, \alpha)\, d\alpha = \Gamma(f - f_0, f_0). \tag{2.19}$$

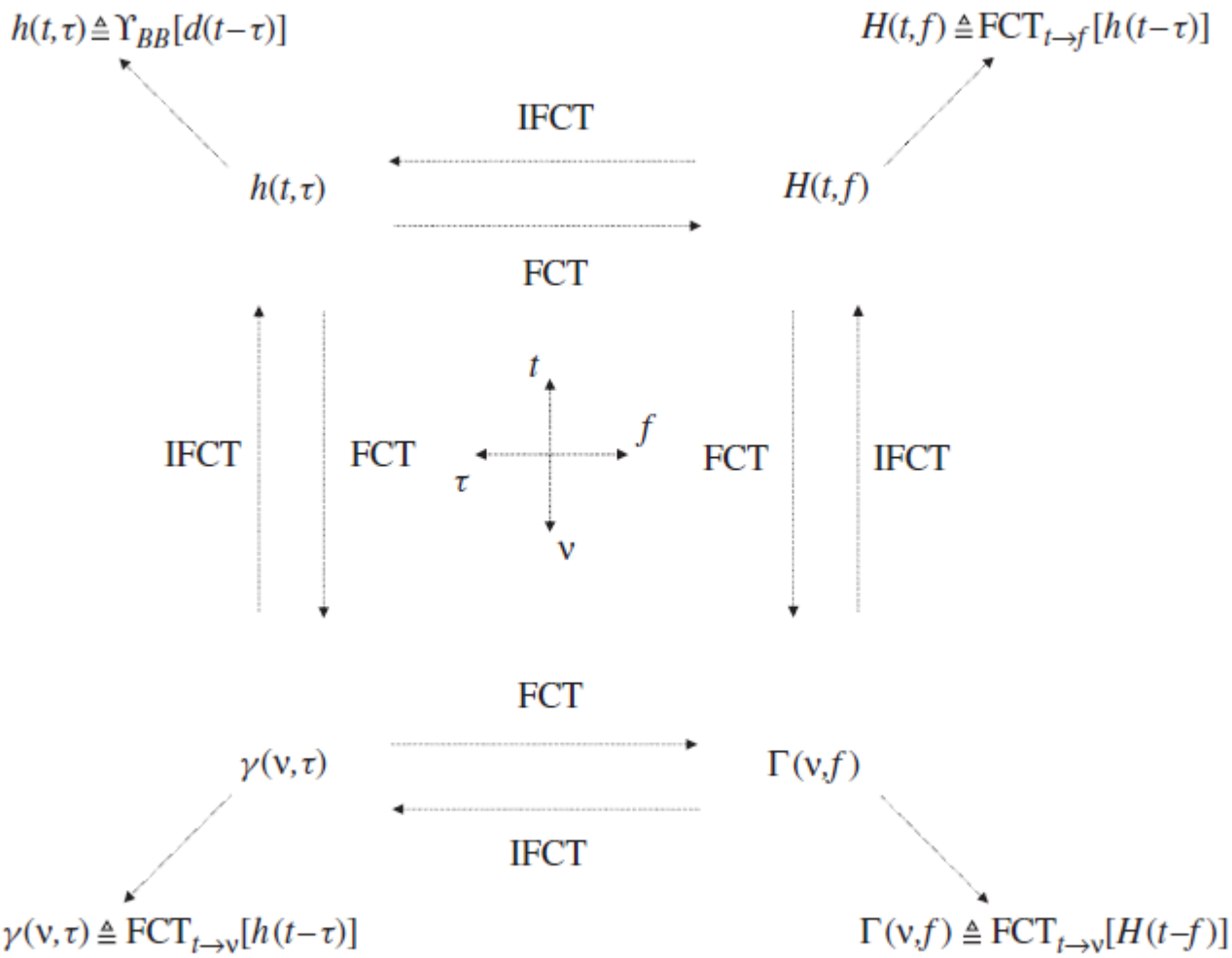

Figure 2.3 Relationships among the four system functions defined in Section 2.2.1.

2.2.1.2 Frequency-Selective Channels

Let us assume that the transmitted signal $x(t)$ has a *finite duration* T_0 and that, within an interval of duration not exceeding T_0, the communication medium does not exhibit any significant change in its physical characteristics. In this case time variability can be neglected and we may represent the channel as a linear and *stationary* system with a CIR $h(\tau)$. For instance, under these assumptions, the L-ray model described in Example 2.2.1 may be characterized by the impulse response[9] (see (2.25))

$$h(\tau) = \sum_{i=0}^{L-1} a_i \, \delta(\tau - \tau_i), \tag{2.29}$$

where the complex gains $\{a_i\}$ are *time-invariant*.

2.2.1.3 Time-Selective Channels

Let us now consider the dual case to that illustrated in Section 2.2.1.2. We now assume that the channel variations are significant within the observation interval[12] and that the reciprocal of the bandwidth B_x of $x(t)$ is *significantly smaller than the time dispersive effect of the channel*, so that, if τ_m denotes the maximum delay as above, then:

$$B_x \ll 1/\tau_m. \tag{2.30}$$

Then, since $h(t, \tau) = 0$ for $\tau < 0$ and $\tau > \tau_m$, (2.9) can be rewritten as:

$$y(t) = \int_0^{\tau_m} x(t - \tau)\, h(t, \tau)\, d\tau. \tag{2.31}$$

From (2.30) it is immediately seen that, in any time interval of duration τ_m, $x(t)$ undergoes only small changes, so that $x(t - \tau) \cong x(t)$ for $0 \leq \tau \leq \tau_m$. Then (2.31) can be approximated as:

$$y(t) = x(t)\, a(t), \tag{2.32}$$

where

$$a(t) \triangleq \int_0^{\tau_m} h(t, \tau)\, d\tau. \tag{2.33}$$

READ Page 39 to 43 *2.2.2 Statistical Characterization of a SISO Wireless Channel*

Table 2.2 Some relevant data for specific PDPs

PDP	$P_h(\tau)$	$R_H(f)$	τ_{ds}
U	$\frac{1}{\tau_0}\{\mathrm{u}(\tau) - \mathrm{u}(\tau - \tau_0)\}$	$\mathrm{sinc}(f\ \tau_0)\ e^{-j\pi f\ \tau_0}$	$\frac{\tau_0}{\sqrt{12}}$
T	$\frac{1}{\tau_0}\left(1 - \frac{\lvert\tau\rvert}{\tau_0}\right)\mathrm{rect}\left(\frac{\tau}{2\tau_0}\right)$	$\mathrm{sinc}^2(f\ \tau_0)$	$\frac{\tau_0}{\sqrt{6}}$
E	$\frac{1}{\tau_0}\ e^{-\tau/\tau_0}\mathrm{u}(\tau)$	$\frac{1}{1 + j2\pi f\ \tau_0}$	τ_0
G	$\frac{1}{\tau_0\sqrt{2\pi}}e^{-\tau^2/2\tau_0^2}$	$e^{-2(\pi f\ \tau_0)^2}$	τ_0
TE	$\frac{e^{-\tau/\tau_0}}{\tau_0(1 - e^{-\tau_M/\tau_0})}[\mathrm{u}(\tau) - \mathrm{u}(\tau - \tau_M)]$	$\frac{1 - e^{-\tau_M/\tau_0 - j2\pi f\tau_M}}{(1 - e^{-\tau_M/\tau_0})(1 + j2\pi f\ \tau_0)}$	eq. (2.53)

channel effects on the two signals can be substantially different. If B_c is defined as the width of the interval over which the normalized autocorrelation function of $H(f)$ does not take values smaller than 0.9, it can be expressed approximately as [6, p. 200]:

$$B_c \cong \frac{1}{50\tau_{\cdot}}. \tag{2.54}$$

in polar form with phase $\Theta \triangleq \angle a(t) \in [0, 2\pi)$ and amplitude $R \triangleq |a(t)|$, it is easy to prove that:

(a) Θ and R are *statistically independent*;
(b) the pdf of Θ is uniform over $(0, 2\pi)$, whereas that of R is:

$$f_R(r) = u(r)\,\frac{r}{\sigma_a^2}\exp\left(-\frac{r^2}{2\sigma_a^2}\right), \tag{2.58}$$

that is, R has a *Rayleigh* distribution [55, p. 200]. For this reason, the case $A = 0$ is usually referred to as that of *Rayleigh fading*.

If we now assume that $A \neq 0$, so that $P_a = A^2 + 2\sigma_a^2$, it can be proved that the phase Θ of $a(\bar{t})$ is no longer uniform and statistically independent of the amplitude R (e.g., see [88, pp. 47–48]) and that R is characterized by the *Rice* pdf[16] [55]:

$$f_R(r) = u(r)\,\frac{r}{\sigma_a^2}\exp\left(-\frac{r^2 + A^2}{2\sigma_a^2}\right) I_0\left(\frac{A\,r}{\sigma_a^2}\right), \tag{2.59}$$

where $I_0(\cdot)$ is the *modified Bessel function* of the first kind and of zero order. In this case it is commonly stated that the channel is affected by *Rician fading*. Note that the condition $A \neq 0$ indicates the presence of a specular (i.e., LOS) component, often present in satellite and terrestrial (typically suburban and rural) scenarios, and that the relevance of the LOS component is described by the ratio of the power of the *deterministic* (LOS) *component* to the average power of the *random component* of $a(t)$, that is, by the parameter:

$$K \triangleq \frac{A^2}{2\sigma_a^2}, \tag{2.60}$$

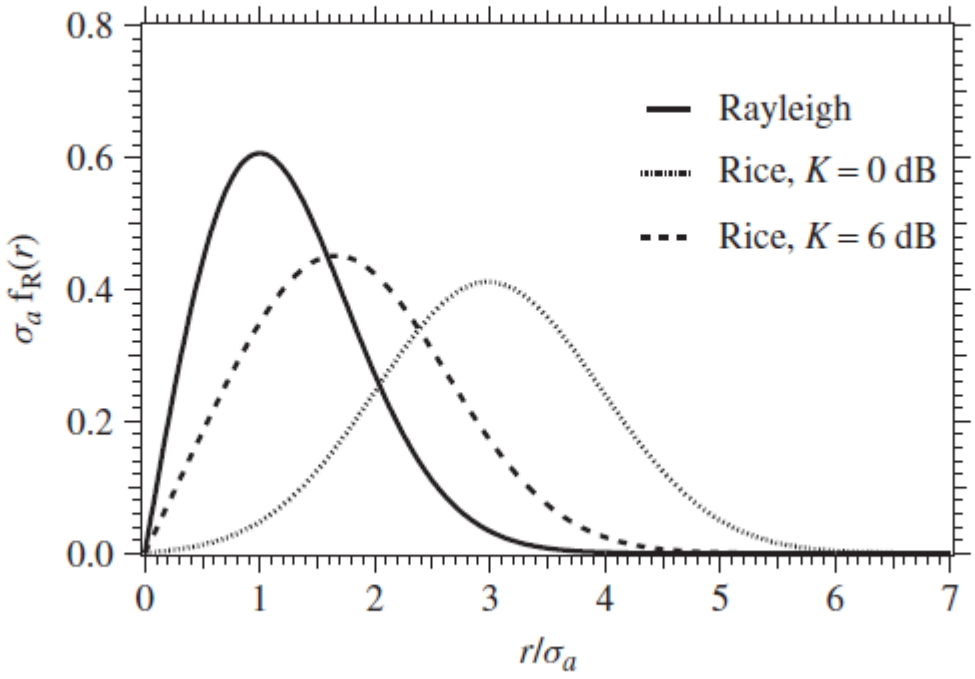

Figure 2.4 Representation of the Rice pdf (2.59) for $K_{dB} = -\infty$, 6 and 0 dB.

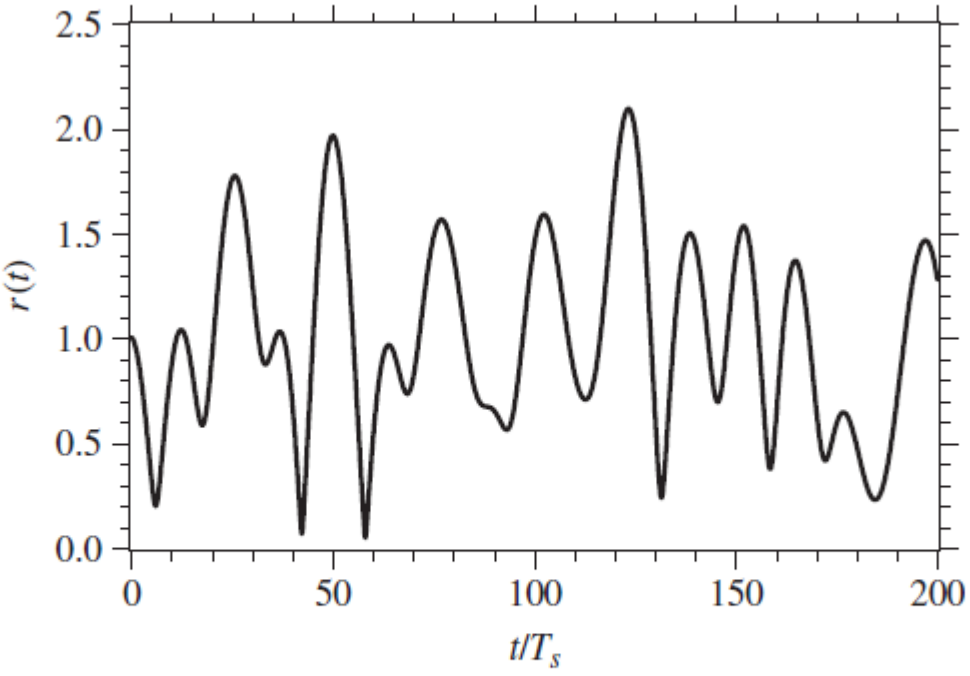

Figure 2.5 Time evolution of the fading amplitude $r(t)$ for a sample function of time-selective fading $a(t)$.

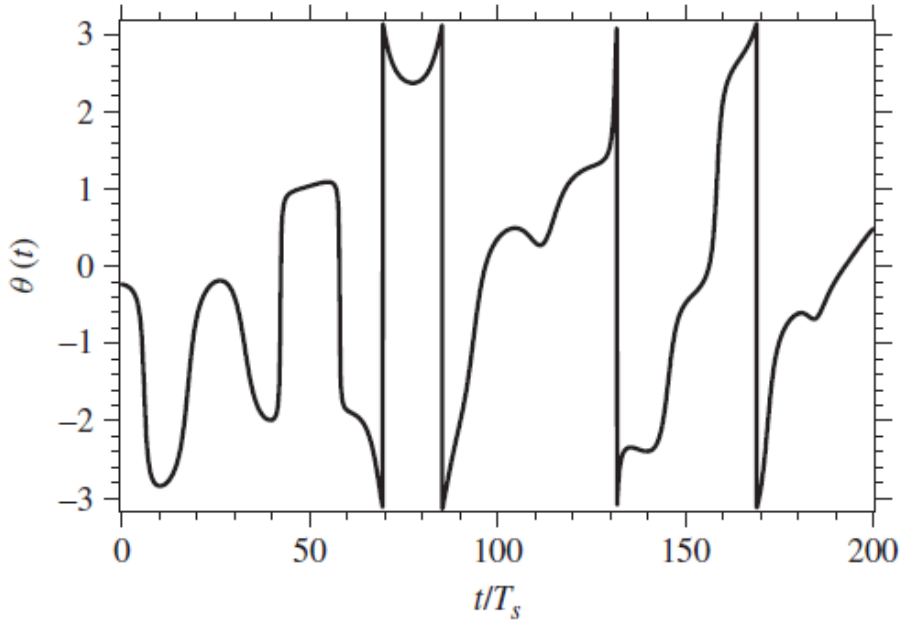

Figure 2.6 Time evolution of the fading phase $\theta(t)$ for a sample function of time-selective fading $a(t)$.

2.2.2.4 Doubly-Selective Channels

In considering time-selective and frequency-selective channels we have primarily been concerned with the channel multiplicative distortion $a(t)$ and the frequency response $H(f)$, respectively, and both system functions have been modeled as *Gaussian random processes*. It is not difficult to understand that, in the doubly-selective case, the property of Gaussianity is preserved for $H(t, f)$, so that a full statistical characterization of this system function is given by its mean value function:

$$H_d(t, f) \triangleq \mathrm{E}\{H(t, f)\} \tag{2.73}$$

and by its autocorrelation function:

$$R_H(t_1, t_2; f_1, f_2) \triangleq \mathrm{E}\{H(t_1, f_1)\ H^*(t_2, f_2)\}, \tag{2.74}$$

called the *time–frequency correlation function*. In the following we focus only on the case of Rayleigh fading, so that knowledge of the second statistic is sufficient for a complete statistical picture.

We now analyze the structure of $R_H(t_1, t_2; f_1, f_2)$ under the US and WSS hypotheses, and that of the autocorrelation functions of $h(t, \tau)$ and $\gamma(\nu, \tau)$ for the same cases. To begin, we note that acquiring an accurate knowledge of $R_H(t_1, t_2; f_1, f_2)$ is not easy, because it depends on four distinct variables, two in the time domain and two in the frequency domain. A substantial simplification in the mathematical structure of this function is introduced, however, if the US and/or WSS properties hold. In fact, if the channel is US (see (2.46)), then:

$$R_H(t_1, t_2; f_1, f_2) = R_H(t_1, t_2; f_1 - f_2); \tag{2.75}$$

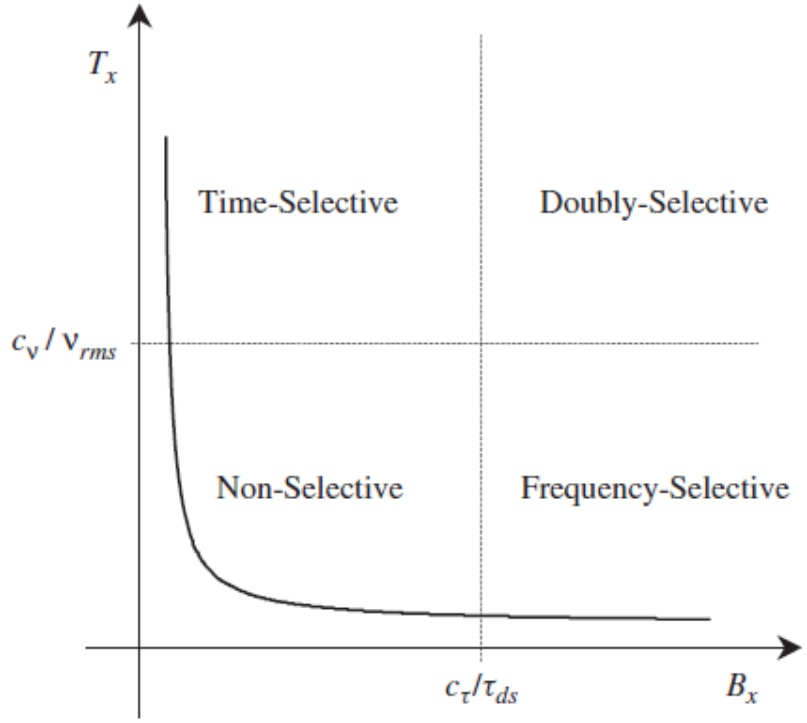

Figure 2.9 Schematic representation, in the bandwidth–duration plane (B_x, T_x) of the transmitted signal, illustrating the effects of fading on wireless communication.

(a) TDL models with equally spaced taps;
(b) *Karhunen–Loève* (KL) models;
(c) models based on polynomial representations of system functions;
(d) models based on the approximation of channel autocorrelation functions via *Gaussian quadrature rules* (GQRs).

2.2.3.2 Tapped Delay Line Model for Bandlimited Signals

This model belongs to the class of the so-called *sampling models*,[23] first devised by T. Kailath in [105, p. 20] and later extended by P. A. Bello in [78]. It is based on the assumption that the channel input signal $x(t)$ has a finite bandwidth B, so that the corresponding channel response $y(t)$ depends on its TVTF $H(f,t)$ for $f \in (-B, B)$ only (see (2.99)), that is, it depends on the function:

$$\hat{H}(t, f) \triangleq H(t, f)[u(f - B) - u(f + B)]. \tag{2.103}$$

Let us define the function:

$$\hat{h}(t, \tau) \triangleq \text{IFCT}_{f \to \tau}[\hat{H}(t, f)] = \int_{-B}^{B} H(t, f) \exp(j2\pi f \tau)\, df \tag{2.104}$$

and note that $\hat{h}(t, \tau)$, being rigorously bandlimited (if its dependence on τ is considered), can be represented via the *sampling theorem* (e.g., see [106, p. 20]) as:

$$\hat{h}(t, \tau) = \sum_{n=-\infty}^{+\infty} \hat{h}\left(t, \frac{n}{2B}\right) \text{sinc}\left(2B\left(\tau - \frac{n}{2B}\right)\right), \tag{2.105}$$

READ Page 57 to 60 Models

2.3.1 Input–Output Characterization of a MIMO Wireless Channel

We now focus on a MIMO communication system having n_R receive and n_T transmit antennas (or an $n_T \times n_R$ MIMO system for short), as illustrated in Figure 2.11. A full description of the input–output behavior of the overall MIMO channel is provided by the CIR set $\{h_{i,j}(t,\tau), i = 0, 1, \ldots, n_T - 1, j = 0, 1, \ldots, n_R - 1\}$, where $h_{i,j}(t,\tau)$ denotes the CIR between the ith transmit and jth receive antenna. In fact, the complex envelope of the useful signal $y_j(t)$ collected at the output of the jth receive antenna (with $j = 0, 1, \ldots, n_R - 1$) can be expressed as the superposition of the contributions from all the transmit antennas, that is, as (see (2.9)):

$$y_j(t) = \sum_{k=0}^{n_T-1} \int_{-\infty}^{+\infty} x_k(t-\tau)\, h_{k,j}(t,\tau)\, d\tau, \tag{2.136}$$

where $x_k(t)$ is the complex envelope of the signal from the kth transmit antenna (with $k = 0, 1, \ldots, n_T - 1$). This can be expressed in a more compact vector form as:

$$\mathbf{y}(t) = \int_{-\infty}^{+\infty} \mathbf{H}(t,\tau)\, \mathbf{x}(t-\tau)\, d\tau, \tag{2.137}$$

where $\mathbf{x}(t) \triangleq [x_0(t), x_1(t), \ldots, x_{n_T-1}(t)]^T$ and $\mathbf{y}(t) \triangleq [y_0(t), y_1(t), \ldots, y_{n_R-1}(t)]^T$ are the transmitted and the received signal vectors, respectively, and $\mathbf{H}(t,\tau)$ is an $n_R \times n_T$ matrix collecting all the elements of the CIR set and whose element on the jth row (with $j = 0, 1, \ldots, n_R - 1$) and on the ith column (with $i = 0, 1, \ldots, n_T - 1$) is $h_{i,j}(t,\tau)$. The vector function $\mathbf{H}(t,\tau)$ provides a full matrix description of a MIMO communication channel, similar to the CIR $h(t,\tau)$ in a SISO scenario.

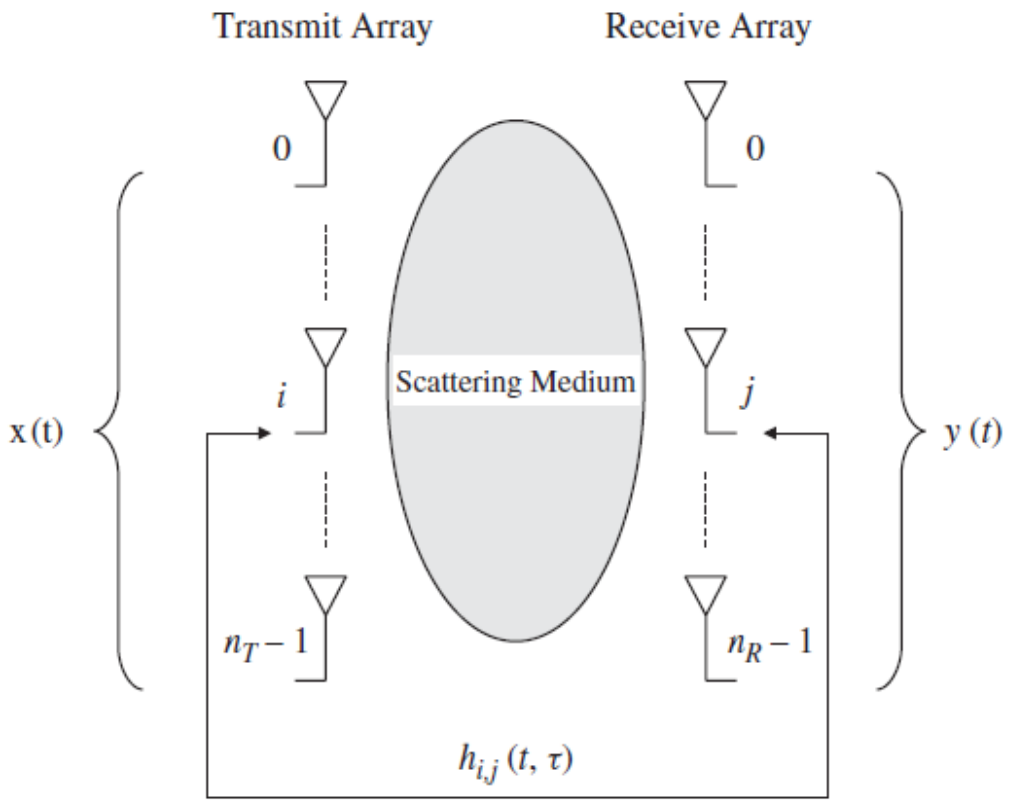

Figure 2.11 MIMO system characterized by n_T transmit and n_R receive antennas. The system function $h_{i,j}(t, \tau)$ denotes the CIR between the ith transmit and jth receive antenna.

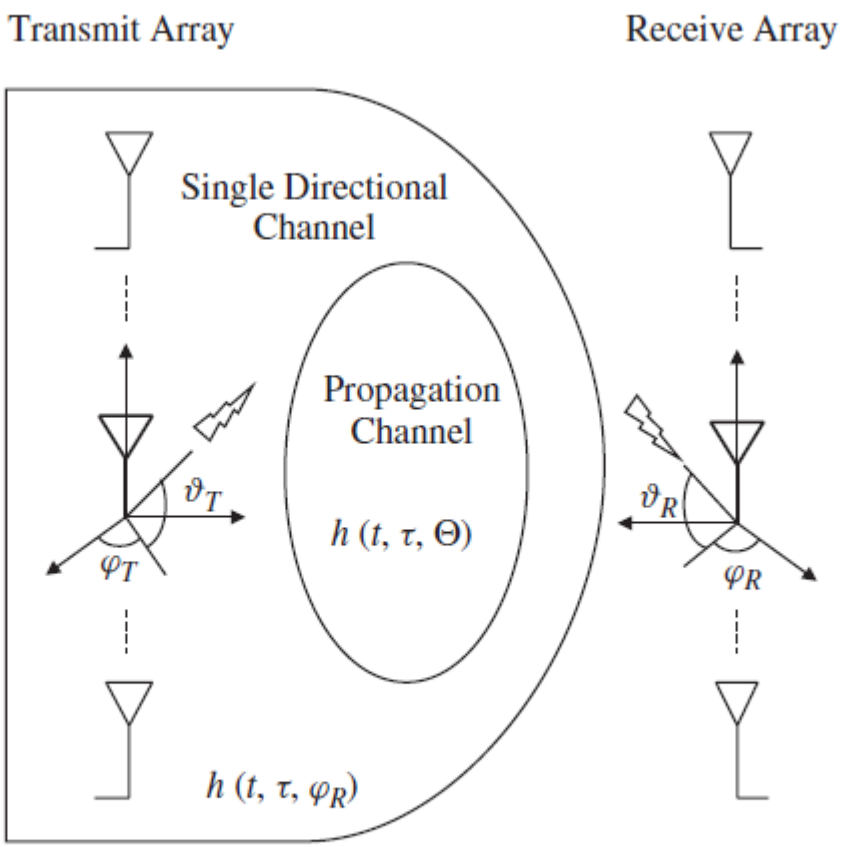

Figure 2.12 Directional description of a propagation scenario in which the transmit/receive arrays of a MIMO communication system operate.

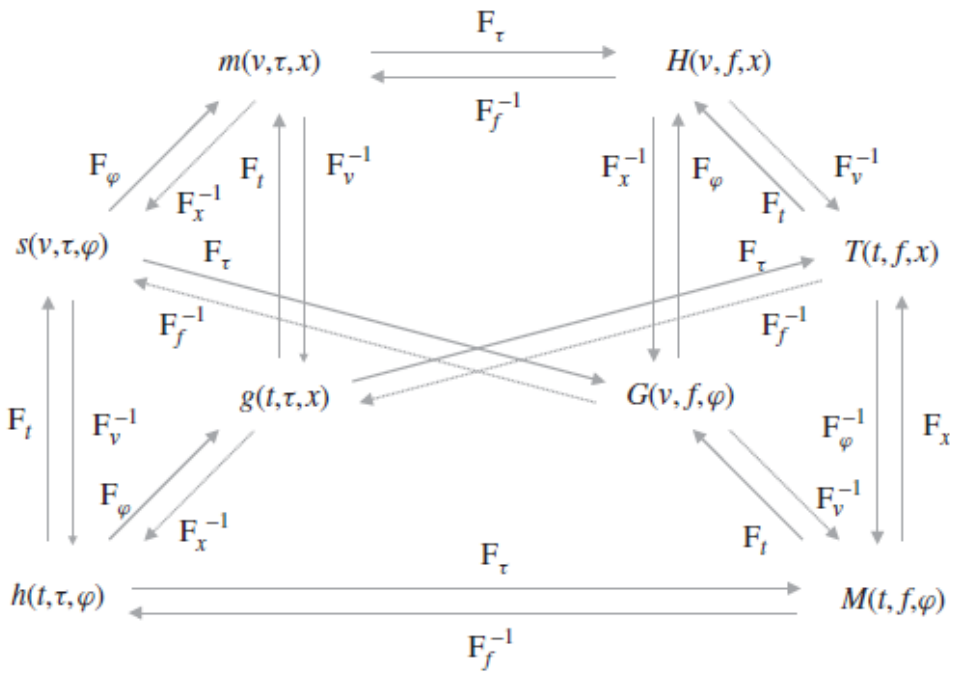

Figure 2.13 Representation of the relationships among the system functions adopted for the directional description of a propagation scenario.

remaining variables. For instance, from $M(t, f, \varphi)$ the *Doppler- and angle-resolved channel transfer function* $G(\nu, f, \varphi) \triangleq \mathrm{TCF}_{t\to\nu}[M(t, f, \varphi)]$ and the *time- and aperture-variant transfer function* $T(t, f, x) \triangleq \mathrm{TCF}_{\varphi\to x}[M(t, f, \varphi)]$ can be derived. Similarly, from $g(t, \tau, x)$ the *Doppler- and aperture-resolved channel impulse response* $m(\nu, \tau, x) \triangleq \mathrm{TCF}_{t\to\nu}[g(t, \tau, x)]$ and, again,

READ Page 66 to 71 Statistics

Page 71 to 80 Models

3 Digital Modulation Techniques

An information-carrying signal, before being transmitted in a communication system, usually undergoes processing, which modifies its characteristics, to make it suitable to send over a given channel. In particular, in digital wireless communications the message consists of a stream of binary data, which is intrinsically a *baseband discrete-time signal*, whereas the communication channel, as illustrated in Chapter 2, can always be modeled as a *passband time-continuous system*. Generally, the transformation of the discrete-time message into a time-continuous signal, having spectral properties suitable for transmission over a given communication channel, is accomplished through a process known as *modulation*.

pulse amplitude modulation (PAM) signals and that
of *continuous phase modulation* (CPM) signals, respectively, are considered.
Then, in Section 3.7, a
specific type of *multicarrier* (MC) signal, known as OFDM, is considered

3.2 General Structure of a Digital Modulator

A *digital modulator* is a device that converts a data sequence to an analog signal suitable for transmission over a physical channel. Here, it is assumed that digital modulators are fed by a WSS sequence $\{d_n\}$, consisting of M-ary data symbols, from some alphabet $A_d = \{0, 1, \ldots, M-1\}$. The data are generated by an information source at a given *signaling* or *symbol rate* $R_s = 1/T_s$, where T_s is the *signaling* or *symbol interval*. A modulator maps d_n, at the instant $t_n = nT_s$, to a *channel symbol* c_n, from an M-ary complex alphabet A_c. Then, the modulator associates $\{c_n\}$ with a baseband signal

$s(t, \mathbf{c})$, which is then up-converted using a *carrier* at frequency f_c, always assumed to be substantially larger than R_s. This generates the RF signal:

$$s_{RF}(t, \mathbf{c}) = \mathrm{Re}\{\, s(t, \mathbf{c}) \;\; \exp\;(j2\pi f_c t)\}, \tag{3.1}$$

where the vector $\mathbf{c} \triangleq [\ldots, c_{-1}, c_0, c_1, \ldots]$, which is generally infinite-dimensional, represents the sequence of channel symbols.

The structure of the data signal $s(t, \mathbf{c})$ can easily be understood if we model its generation using a *finite-state sequential machine* (FSSM), whose inner state, for the modulation formats analyzed in what follows, is always defined by a finite set of discrete parameters. However, as shown in the following pages, it can be always represented by a single integer parameter; for this reason, the modulator state Δ_n at the beginning of the nth signaling interval can take one of N_s possible values, belonging to the alphabet $A_{st} = \{0, 1, \ldots, N_s - 1\}$. At the instant $t_n = nT_s$ the modulator, on the basis of the *present* channel symbol c_n and the *present* state Δ_n, generates the signal $s(\Delta_n, c_n; t - nT_s)$, where $s(\Delta_n, c_n; t)$ belongs to a signal alphabet $A_s = \{s_k(t), k = 0, 1, \ldots, N_w - 1\}$, consisting of $N_w \triangleq M \cdot N_s$ distinct functions, all having *finite energy*. Generally speaking, each of these functions has an arbitrary duration and takes on complex values.

The baseband signal $s(t, \mathbf{c})$ is given by the superposition of the waveforms $\{s(\Delta_n, c_n; t - nT_s)\}$, generated during consecutive symbol intervals as:

$$s(t, \mathbf{c}) = \sum_{n=-\infty}^{+\infty} s(\Delta_n, c_n; t - nT_s), \tag{3.2}$$

which expresses the *output equation* of the FSSM. Note that complete knowledge of the modulator behavior also requires knowledge of the *state equation*, that is, of the mathematical law:

$$\Delta_{n+1} = f(\Delta_n, c_n), \tag{3.3}$$

Let us now assume that the modulator has a *single* state ($N_s = 1$) and that, consequently, it can select one of $N_w = M$ possible waveforms at the beginning of each symbol interval. In this case the signal $s(\Delta_n, c_n; t)$ depends on the present symbol c_n only, so that (3.2) simplifies to:

$$s(t, \mathbf{c}) = \sum_{n=-\infty}^{+\infty} s(c_n; t - nT_s). \tag{3.4}$$

In addition, if all the signals of the set A_s have time support within the interval $[0, T_s)$, the modulator is *memoryless* [32], since, for any n, the signal generated in the nth symbol interval, $[nT_s,(n + 1)T_s)$, depends only on the present symbol c_n.

It should also be noted that equations (3.1)–(3.4) describe the behavior of a digital modulator in *deterministic* terms. In practice, as already stated above, the data sequence $\{d_n\}$ is random, so that the state sequence $\{\Delta_n\}$ is a *discrete-time random process* belonging, if the data $\{d_n\}$ are statistically *independent*, to the class of so-called *Markov chains* [55, 279]; moreover, the signals $s_{RF}(t, \mathbf{c})$ (3.1) and $s(t, \mathbf{c})$ (3.2) (and (3.4)) are *time-continuous stochastic processes*.

When implementing a digital modulator whose behavior can be described as above, it is useful to note that the RF transmitted signal $s_{RF}(t, \mathbf{c})$ (3.1) can be rewritten as:

$$s_{RF}(t, \mathbf{c}) = s_I(t, \mathbf{c})\ \cos(2\pi f_c t) - s_Q(t, \mathbf{c})\ \sin(2\pi f_c t), \tag{3.5}$$

where its *in-phase component*:

$$s_I(t, \mathbf{c}) \triangleq \mathrm{Re}\,\{s(t, \mathbf{c})\} \tag{3.6}$$

and its *quadrature component*:

$$s_Q(t, \mathbf{c}) \triangleq \mathrm{Im}\,\{s(t, \mathbf{c})\} \tag{3.7}$$

because of the limited energy resources available for transmission, highly efficient (and, consequently, *nonlinear*) power amplifiers. In this case the fluctuations of the *envelope*:

$$s_{env}(t, \mathbf{c}) \triangleq |s(t, \mathbf{c})| = \sqrt{s_I^2(t, \mathbf{c}) + s_Q^2(t, \mathbf{c})} \tag{3.8}$$

of the modulated signal $s_{RF}(t, \mathbf{c})$ (3.1) (or, equivalently, (3.5)) become relevant. In fact, a *constant envelope* modulation (or, at least, a modulation with small fluctuations in its envelope) represents an important factor in the above selection process.

To suitably define bandwidth, first note that the cardinality M of the alphabet A_d is usually an integer power of 2 (i.e., $M = 2^m$), so that the data $\{d_n\}$ input to the modulator must be put in one-to-one correspondence with the set of all the possible vectors consisting of m binary digits. Then, the *bit interval* T_b becomes[2]:

$$T_b \triangleq \frac{T_s}{m} = \frac{T_s}{\log M} \tag{3.9}$$

and, consequently, the *bit rate* R_b is given by:

$$R_b \triangleq \frac{1}{T_b}. \tag{3.10}$$

Since $R_s \triangleq 1/T_s$, from (3.9) and (3.10) it is easy to see that:

$$R_b = mR_s = R_s \log M. \tag{3.11}$$

frequency interval.

To suitably define bandwidth, first note that the cardinality M of the alphabet A_d is usually an integer power of 2 (i.e., $M = 2^m$), so that the data $\{d_n\}$ input to the modulator must be put in one-to-one correspondence with the set of all the possible vectors consisting of m binary digits. Then, the *bit interval* T_b becomes[2]:

$$T_b \triangleq \frac{T_s}{m} = \frac{T_s}{\log M} \tag{3.9}$$

and, consequently, the *bit rate* R_b is given by:

$$R_b \triangleq \frac{1}{T_b}. \tag{3.10}$$

Since $R_s \triangleq 1/T_s$, from (3.9) and (3.10) it is easy to see that:

$$R_b = mR_s = R_s \log M. \tag{3.11}$$

In assessing the *energy efficiency* of a digital communication technique, a significant role is played by the parameter E_b, representing the *average energy consumption required for the transmission of a single information bit*. This parameter can be easily related to the average energy E_s spent by a digital modulator in a symbol interval to generate $s_{RF}(t, \mathbf{c})$. Since in each symbol interval $m = \log M$ bits are transmitted, we have that[3]:

$$E_b = \frac{E_s}{m} = \frac{E_s}{\log M}. \tag{3.12}$$

Using these quantities, we will establish appropriate bandwidth measures in Section 3.4.

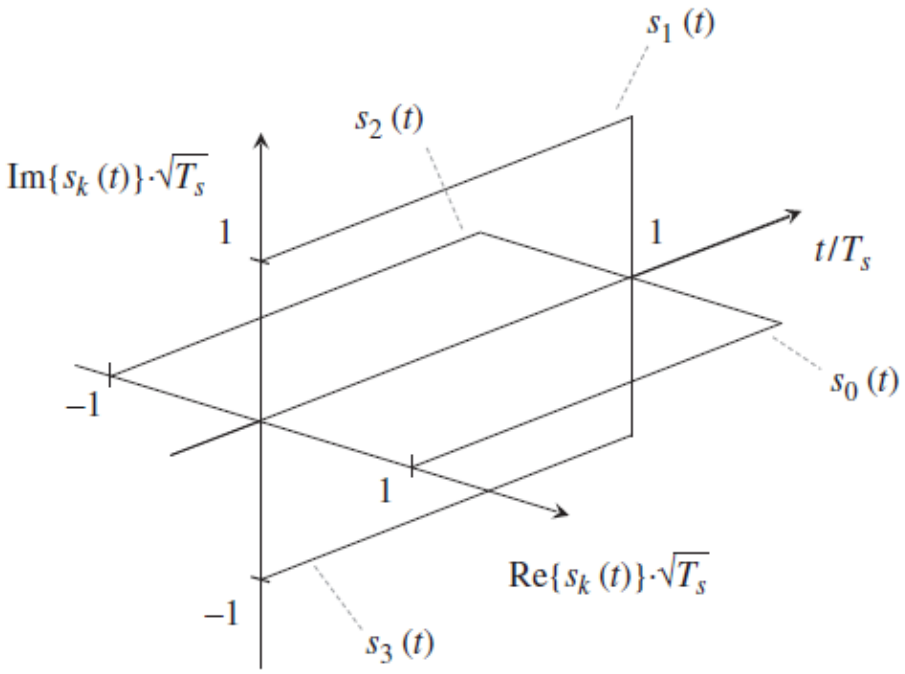

Figure 3.1 Graphical representation of the complex signals $\{s_k(t)\}$ (3.16) in the case of a quaternary alphabet ($M = 4$).

3.4 Bandwidth of Digital Modulations

The signals generated by the digital modulators described in this chapter are *wide-sense cyclostationary* (WSC) random processes with a period T_{cs} (see Appendix B), which is always a multiple of the symbol interval T_s. Therefore, given the modulated signal $s_{RF}(t, \mathbf{c})$ (3.1), characterized by a random

[4] Further details on this modulation format can be found in Section 3.5.2.

symbol vector $\mathbf{c}$ (whose elements belong to an M-ary constellation), a carrier frequency f_c and the complex envelope $s(t, \mathbf{c})$, its *average power spectral density* $S_{RF}(f)$ is given by:

$$S_{RF}(f) = \frac{1}{4}[S_s(f + f_c) + S_s(f - f_c)], \tag{3.24}$$

where $S_s(f)$ is the average *power spectral density* (PSD) of the complex envelope $s(t, \mathbf{c})$. The latter function is the FCT of the *average autocorrelation function* $R_s(\tau)$, that is:

$$S_s(f) = \int_{-\infty}^{+\infty} R_s(\tau)\ \exp\ (-j2\pi f\tau)\, d\tau, \tag{3.25}$$

$$S_{RF}(f) = \frac{1}{4}[S_s(f + f_c) + S_s(f - f_c)], \tag{3.24}$$

where $S_s(f)$ is the average *power spectral density* (PSD) of the complex envelope $s(t, \mathbf{c})$. The latter function is the FCT of the *average autocorrelation function* $R_s(\tau)$, that is:

$$S_s(f) = \int_{-\infty}^{+\infty} R_s(\tau)\ \exp\ (-j2\pi f\tau)\ d\tau, \tag{3.25}$$

with

$$R_s(\tau) \triangleq \frac{1}{T_{cs}} \int_0^{T_{cs}} R_s(t, \tau)\ dt \tag{3.26}$$

and

$$R_s(t, \tau) \triangleq \mathrm{E}\{s(t + \tau, \mathbf{c})\ s^*(t, \mathbf{c})\}. \tag{3.27}$$

Note that the only random quantities in (3.1) are the channel symbols $\{c_n\}$, so that the statistical average (denoted by the operator $\mathrm{E}\{\cdot\}$) required in the computation of $R_s(t, \tau)$ according to (3.27) involves only these.

The average power P_{RF} of the RF signal $s_{RF}(t, \mathbf{c})$ (3.1) is given by:

$$P_{RF} = \int_{-\infty}^{+\infty} S_{RF}(f)\ df, \tag{3.28}$$

so that on substituting (3.24) into (3.28) it is found that:

$$P_{RF} = \frac{P_s}{2}, \tag{3.29}$$

where

$$P_s = \int_{-\infty}^{+\infty} S_s(f)\ df \tag{3.30}$$

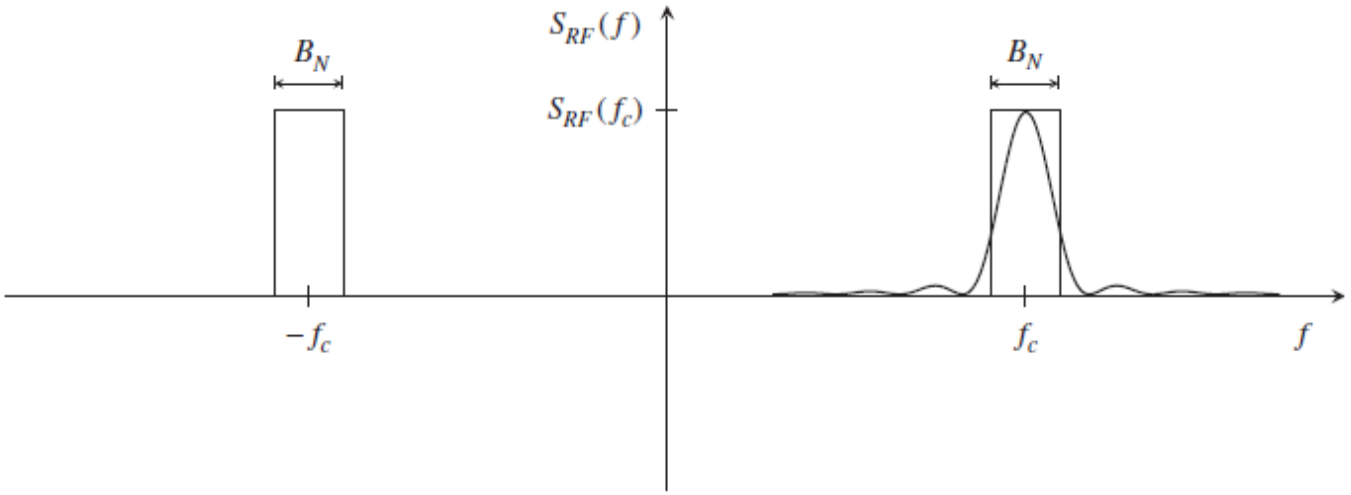

Figure 3.2 Geometrical interpretation of equality (3.35). The parameter B_N represents the equivalent noise bandwidth of a digital signal characterized by the PSD $S_{RF}(f)$, plotted on a linear scale.

generated by the time translations of B_s with a delay equal to iT_s seconds ($i = 0, 1, \ldots, P-1$) be *mutually orthogonal*. From a mathematical viewpoint this requires the generation of a set of PD orthogonal functions which are bandlimited to B Hertz and whose energy is primarily concentrated in an interval of duration PT_s seconds. Then substituting for the parameters N and T_0 with PD and PT_s, respectively, in (3.41) yields:

$$D \leq 2BT_s, \tag{3.42}$$

from which it can be inferred that:

$$B \geq \frac{D}{2T_s}. \tag{3.43}$$

If we now define the parameter:

$$D_b = \frac{D}{\log M}, \tag{3.44}$$

representing the number of dimensions employed for a transmitted bit, (3.43) can be rewritten as:

$$B \geq \frac{D_b R_b}{2}. \tag{3.45}$$

This leads to the estimate of the minimum bandwidth:

$$B_{\min} = \frac{D_b R_b}{2} \tag{3.46}$$

required by a digital signal employing D_b dimensions per bit and occurring at a rate R_b. This result, even if not exact, is significant, as it shows the importance of using modulation formats characterized by small values of D_b when limited bandwidth occupancy is required. Finally, we note that equation (3.45) can be used for both baseband and passband transmissions, but *real signals* must be always considered in the evaluation[9] of D_b.

READ Page 90 to 146

3.5 Passband PAM
3.5.1 Signal Model

3.6 Continuous Phase Modulation
3.6.1 Signal Model

3.7 OFDM

3.7.2 OFDM Signal Model

3.9 Spectral Properties of a Digital Modulation at the Output of a Wireless Channel

In this section the mathematical tools described in Section 3.4 and some results derived in Chapter 2 are applied to the analysis of the spectral properties of a digital modulation transmitted through a doubly-selective wireless channel. This allows us to assess the effects of time selectivity in the frequency domain and to establish a relationship between the average *received* energy per symbol interval and the average energy *transmitted* in the same interval.

In our analysis it is assumed that: (a) the complex envelope $s(t, \mathbf{c})$ of the transmitted signal depends on a random vector $\mathbf{c}$ of channel symbols and is WSC with period T_{cs}; and (b) the CIR $h(t, \tau)$ is *statistically independent* of $s(t, \mathbf{c})$. Then, the useful component of the channel response to $s(t, \mathbf{c})$ is (see (2.9)):

$$z(t, \mathbf{c}) \triangleq \int_{-\infty}^{+\infty} s(t - \tau, \mathbf{c})\, h(t, \tau)\, d\tau, \tag{3.347}$$

so that the autocorrelation function of $z(t, \mathbf{c})$ is given by:

$$\begin{aligned} R_z(t, \tau) &\triangleq \mathrm{E}\{z(t + \tau, \mathbf{c})\, z^*(t, \mathbf{c})\} \\ &= \int_{\alpha=-\infty}^{+\infty} \int_{\beta=-\infty}^{+\infty} R_s(t - \beta, \tau + \beta - \alpha)\, R_h(t + \tau, t; \alpha, \beta)\, d\beta\, d\alpha, \end{aligned} \tag{3.348}$$

$$R_z(\tau) \triangleq \frac{1}{T_{cs}} \int_0^{T_{cs}} R_z(t,\tau)\, dt$$
$$= \frac{1}{T_{cs}} \int_{t=0}^{T_{cs}} \int_{\alpha=-\infty}^{+\infty} R_s(t-\alpha,\tau)\; P_h(\tau;\alpha)\; d\alpha\; dt. \tag{3.350}$$

If on the RHS of the latter equation the integration order is reversed and we note that:

$$\frac{1}{T_{cs}} \int_{t=0}^{T_{cs}} R_s(t-\alpha,\tau)\; dt = R_s(\tau) \tag{3.351}$$

for any α, where $R_s(\tau)$ is the average autocorrelation function of $s(t,\mathbf{c})$, it is found that:

$$R_z(\tau) = R_s(\tau) \int_{-\infty}^{+\infty} P_h(\tau;\alpha)\; d\alpha. \tag{3.352}$$

Moreover, if we assume that $P_h(\tau;\alpha)$ is separable, that is, that $P_h(\tau;\alpha) = R_D(\tau)\; P_h(\alpha)$ (see (2.95)), where $R_D(\tau)$ (with $R_D(0) = 1$) is the *Doppler autocorrelation function* and $P_h(\tau)$ is the channel PDP, (3.352) can be rewritten as:

$$R_z(\tau) = R_s(\tau)\; R_D(\tau) \int_{-\infty}^{+\infty} P_h(\alpha)\; d\alpha. \tag{3.353}$$

This result shows that, if the channel PDP is *normalized*, that is, if:

$$\int_{-\infty}^{+\infty} P_h(\alpha)\; d\alpha = 1, \tag{3.354}$$

then $z(t,\mathbf{c})$ in (3.347) is characterized by the average autocorrelation function:

$$R_z(\tau) = R_s(\tau)\; R_D(\tau) \tag{3.355}$$

and, consequently, by the average PSD:

$$S_z(f) \triangleq \mathrm{FCT}[R_z(\tau)] = S_s(f)\; \otimes S_D(f) = \int_{-\infty}^{+\infty} S_s(\alpha)\; S_D(f-\alpha)\; d\alpha, \tag{3.356}$$

3.7.3 Power Spectral Density of OFDM

In this subsection a closed-form expression for the power spectral density of an OFDM signal is derived under the assumptions that the channel symbols $\{c_n^{(l)}\}$ are iid, and have zero mean (to avoid the presence of spectral lines [28]) and variance $\sigma_c^2 \triangleq \mathrm{E}\{|c_n^{(l)}|^2\}$. To begin, we note that the structure of the signal $s(t, \mathbf{c})$ (3.274) is similar to that of a PAM signal, as already pointed out in Section 3.7.2.2. From a statistical viewpoint, however, there is a fundamental difference between them, since the data sequence $\{a_k^{(l)}\}$ feeding the transmitter filter in the OFDM case is not WSS, but WSC with period $N_T \triangleq N + N_p$. This implies that $s(t, \mathbf{c})$ (3.274) is also WSC with period $T_{cs} = N_T T_s$. Note that the cyclostationarity of the OFDM data sequence is not at all surprising, since, in an OFDM system, data transmission is accomplished on a block-by-block basis and each block has a duration equal to N_T. For a PAM signal characterized by a WSC data sequence, it can be proved [28] that expression (3.66) still holds, provided that $\bar{S}_c(f)$ denotes the *average power spectrum* of the data sequence $\{a_k^{(l)}\}$, that is, the Fourier transform of its *average autocorrelation function*. For this reason, the evaluation of the power spectral density for an OFDM signal proceeds via the following steps: (a) evaluation of the latter function; (b) evaluation of the former function via Fourier methods; (c) application of (3.66) to the evaluation of the power spectral density of an OFDM signal.

3.7.3.2 Evaluation of the Average Power Spectral Density of $\{b_k\}$

The *average power spectral density* $\bar{S}_b(f)$ of $\{b_k\}$ is the Fourier transform of the sequence $R_b[n]$ in (3.290). Since the Fourier transform of the sequence $g[k]$ in (3.291) is:

$$\bar{G}(f) = \frac{1}{NN_T} \frac{\sin^2(\pi N_T f T_s)}{\sin^2(\pi f T_s)}, \tag{3.293}$$

3.8 Lattice-Based Multidimensional Modulations

In Section 3.3 it was shown how the representation, in terms of an orthonormal basis, of the signal alphabet A_s, generated by a given digital modulator in baseband, leads to a new set, consisting of N_w multidimensional points and known as a *constellation*. Most passband PAM constellations (see Section 3.5.2) are characterized by a *regular* placement of their points, since regularity simplifies both signal generation and detection. For this reason, generally speaking, most known signal constellations are generated by extracting their points from a proper *lattice*, that is from a *set of points placed in a regular fashion in a multidimensional space*. Note that the study of the possible signal constellations inevitably leads to an examination of the problem of their *optimality*. An M-ary constellation can be deemed *optimal* if, for a given error performance, it minimizes the *average energy per information bit* required to achieve this target. If the communication channel introduces *additive white Gaussian noise* (AWGN) only, the error performance of a digital receiver at large SNRs depends only on the *minimum distance* between constellation points [321]. In addition, signal space theory shows that the average energy expense decreases as the density of points around the origin increases. For this reason, an M-ary constellation is *optimal* for AWGN channel signaling if it consists of a set of M points that, for an assigned minimum distance among adjacent points, are placed in the *densest* possible way around the origin. The design of optimal constellations leads to the well-known *sphere-packing problem* [322, 323], whose solution leads to an algorithm that allows the placing of a set of equal N-dimensional spheres according to the *densest* possible geometry.

The aim of this section is to provide the basics of lattice theory. The main algebraic and geometric properties of lattices are outlined and some construction methods described. This material is necessary for the later discussion of *signal space codes* in Chapter 11.

3.8.1 Lattices: Basic Definitions and Properties

A *real lattice* Λ is a discrete set of points $\boldsymbol{\lambda}$ belonging to a real Euclidean n-dimensional space $\mathbb{R}^n$ and forming a *group* under the vector addition operator (see Appendix E). In principle, the vectors in a lattice Λ span $d \leq n$ dimensions; however, all the lattices considered in this book are characterized by $d = n$, that is, their vectors span exactly n dimensions. For this reason, in what follows we will call a lattice of real n-tuples an n-dimensional real lattice. Generally speaking, the points of an n-dimensional real lattice Λ are arranged in a regular fashion and are described by a set of d-dimensional linearly independent row vectors $\{\mathbf{g}_l, l = 0, 1, \ldots, n-1\}$, called *generators*, such that:

$$\Lambda \triangleq \{\boldsymbol{\lambda} | \boldsymbol{\lambda} = \mathbf{i}_n \, \mathbf{G}_\Lambda = i_0 \mathbf{g}_0 + i_1 \mathbf{g}_1 + \ldots + i_{d-1} \mathbf{g}_{n-1}\}, \tag{3.312}$$

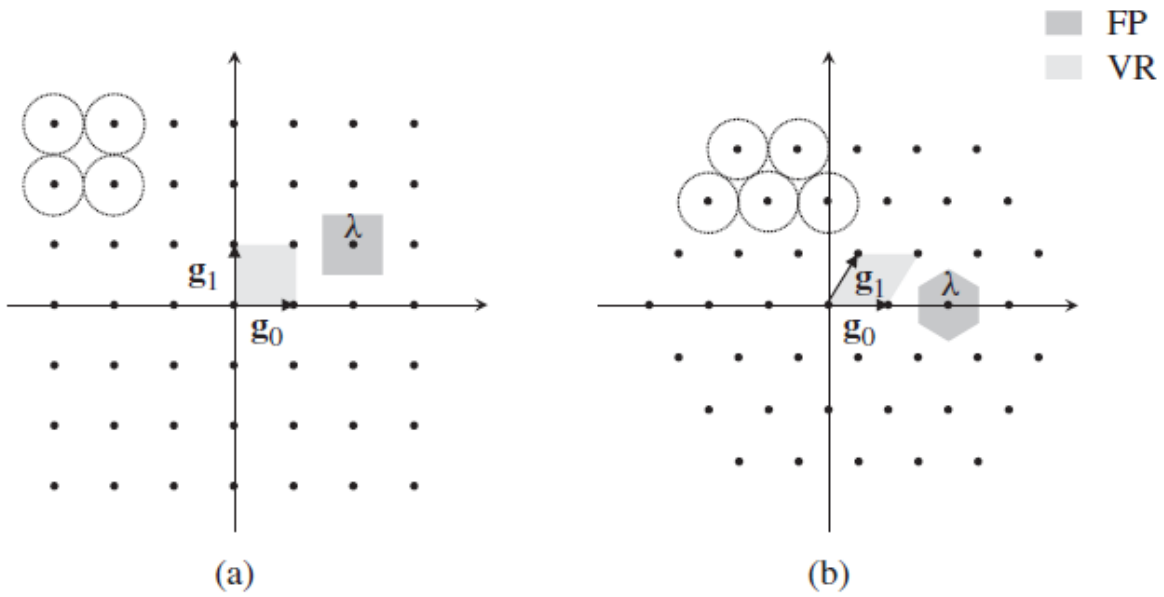

Figure 3.41 Two-dimensional lattices $\mathbb{Z}^2$ and $\mathcal{A}_2$: illustration of generators $\{\mathbf{g}_0, \mathbf{g}_1\}$, sphere packing, *fundamental parallelotopes* (FPs) and *Voronoi regions* (VRs) of a lattice point $\boldsymbol{\lambda}$.

3.9 Spectral Properties of a Digital Modulation at the Output of a Wireless Channel

In this section the mathematical tools described in Section 3.4 and some results derived in Chapter 2 are applied to the analysis of the spectral properties of a digital modulation transmitted through a doubly-selective wireless channel. This allows us to assess the effects of time selectivity in the frequency domain and to establish a relationship between the average *received* energy per symbol interval and the average energy *transmitted* in the same interval.

In our analysis it is assumed that: (a) the complex envelope $s(t, \mathbf{c})$ of the transmitted signal depends on a random vector $\mathbf{c}$ of channel symbols and is WSC with period T_{cs}; and (b) the CIR $h(t, \tau)$ is *statistically independent* of $s(t, \mathbf{c})$. Then, the useful component of the channel response to $s(t, \mathbf{c})$ is (see (2.9)):

$$z(t, \mathbf{c}) \triangleq \int_{-\infty}^{+\infty} s(t - \tau, \mathbf{c})\, h(t, \tau)\, d\tau, \tag{3.347}$$

so that the autocorrelation function of $z(t, \mathbf{c})$ is given by:

$$\begin{aligned} R_z(t, \tau) &\triangleq \mathrm{E}\{z(t + \tau, \mathbf{c})\, z^*(t, \mathbf{c})\} \\ &= \int_{\alpha=-\infty}^{+\infty} \int_{\beta=-\infty}^{+\infty} R_s(t - \beta, \tau + \beta - \alpha)\, R_h(t + \tau, t; \alpha, \beta)\, d\beta\, d\alpha, \end{aligned} \tag{3.348}$$

Read Page 167 *3.10.2 CPM Signaling*

Detection of Digital Signals over Wireless Channels: Decision Rules

4.1 Introduction

Any digital receiver employs a specific *detection strategy* or algorithm for estimating the message transmitted by a given source from a received set of information-bearing noisy data. This is extracted from a single or multiple received waveforms by means of filtering and sampling operations, and is processed by the detection algorithm to generate a set of real quantities, called *detection metrics*. Each value of this metric is associated with a specific *hypothesis* about the transmitted message and is used by the receiver to make decisions on the basis of a mapping rule, which maps values of the metric to messages. In most instances, the hypothesis associated with the best (e.g., the minimum or maximum) metric is selected.

This chapter is devoted to the study of the following two problems:

(a) how a finite set of data (i.e., a finite-dimensional vector) can be extracted from a continuous-time received waveform for the purpose of accomplishing data detection,
(b) how detection metrics can be formulated for the digital modulation techniques described in Chapter 3 in a fading multipath channel scenario.

In particular, in our analysis we focus on the *maximum a posteriori probability* (MAP) and the *maximum likelihood* (ML) detection strategies. These process a finite-dimensional vector of received samples to generate a set of detection metrics, on the basis of which an optimal decision about the transmitted message can be taken. However, the exploitation of these strategies in a real-world digital receiver requires the extraction of a finite-dimensional vector of noisy data from the received waveform. This problem is analyzed in Section 4.4, where it is tackled first from a general perspective. Then the structure of this vector is illustrated for different modulation formats. In Section 4.5 the mathematical tools developed in Section 4.3 are exploited to develop optimal decision metrics for the following cases:

(a) CIR ideally known at the receiver;
(b) CIR known only statistically at the receiver;
(c) unknown CIR.

In particular, metrics for ML *sequence detection* (MLSD), MAP *symbol detection* (MAPSD), and MAP *bit detection* (MAPBD) are derived. In addition, on the basis of these metrics, some general performance bounds are derived.

4.2 Wireless Digital Communication Systems: Modeling, Receiver Architecture and Discretization of the Received Signal

In this section a general model of a wireless communication system is first developed. Then some details about the receiver structure are provided, primarily dealing with the receiver front-end.

4.2.1 General Model of a Wireless Communication System

A general model for an uncoded SISO wireless digital communication system is illustrated in Figure 4.1. A discrete information source generates a message m, belonging to the finite alphabet $A_m = \{m_i, i = 0, 1, \ldots, N_m - 1\}$, having cardinality N_m and whose ith element is characterized by the *a priori probability* $P_i \triangleq \Pr\{m = m_i\}$ (for $i = 0, 1, \ldots, N_m - 1$). In general, each message can be associated with one or more bits generated by a source and can be represented by one or more channel symbols (see Section 3.2), as will become clearer in what follows. The source feeds the digital modulator, which maps m into a finite-dimensional vector $\mathbf{c}$ of channel symbols (via a one-to-one mapping) and then generates the complex baseband signal $s(t, \mathbf{c})$. In doing so, the modulator adopts the finite alphabet $A_s = \{s_i(t) = s(t, \mathbf{c}^{(i)}), i = 0, 1, \ldots, N_m - 1\}$, having the same cardinality as A_m, where $\mathbf{c}^{(i)}$ denotes the ith possible value of $\mathbf{c}$. To simplify the notation, in what follows we will always assume that the one-to-one correspondence:

$$s(t, \mathbf{c}) = s_i(t) \Leftrightarrow m = m_i, \tag{4.1}$$

holds, namely, that the modulator-generated signal $s_i(t)$ is in response to m_i, with $i = 0, 1, \ldots, N_m - 1$. Note that, unlike Chapter 3, here the dependence on m_i is shown by the signal subscript

4.2.2 Receiver Architectures

On the basis of the type of front-end processing employed, radio receivers can be classified into two categories: *direct-conversion* (*homodyne*) and *superheterodyne* receivers. Their architectures are illustrated in Figures 4.2 and 4.3, respectively. In a direct-conversion receiver [416] the received RF signal $r_{RF}(t)$ undergoes filtering (to remove out-of-band noise and interference) and low-noise amplification to reduce the overall noise figure. The RF filter output is sent to two mixers which are also fed by two quadrature oscillations generated by a local oscillator locked to the carrier frequency f_c. The mixer outputs feed two distinct baseband filters that remove residual out-of-band noise and interference, and to avoid aliasing which may originate from sampling their outputs. The outputs of the baseband filters undergo *analog-to-digital* (A/D) conversion and further baseband processing to extract the transmitted data.

4.2.2 Receiver Architectures

On the basis of the type of front-end processing employed, radio receivers can be classified into two categories: *direct-conversion* (*homodyne*) and *superheterodyne* receivers. Their architectures are illustrated in Figures 4.2 and 4.3, respectively. In a direct-conversion receiver [416] the received RF signal $r_{RF}(t)$ undergoes filtering (to remove out-of-band noise and interference) and low-noise amplification to reduce the overall noise figure. The RF filter output is sent to two mixers which are also fed by two quadrature oscillations generated by a local oscillator locked to the carrier frequency f_c. The mixer outputs feed two distinct baseband filters that remove residual out-of-band noise and interference, and to avoid aliasing which may originate from sampling their outputs. The outputs of the baseband filters undergo *analog-to-digital* (A/D) conversion and further baseband processing to extract the transmitted data.

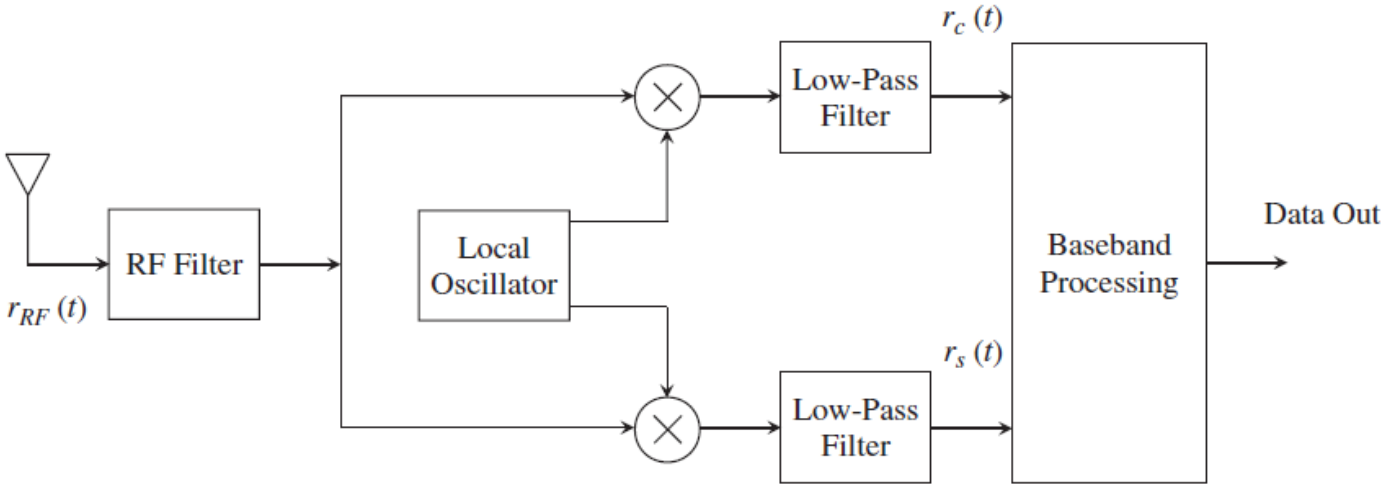

Figure 4.2 Architecture of a direct-conversion receiver.

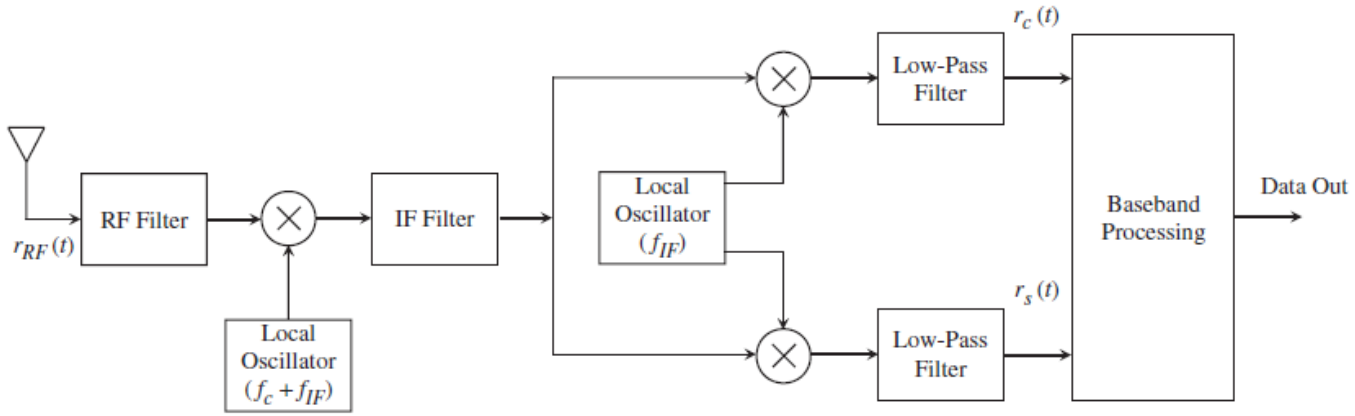

Figure 4.3 Architecture of a superheterodyne receiver.

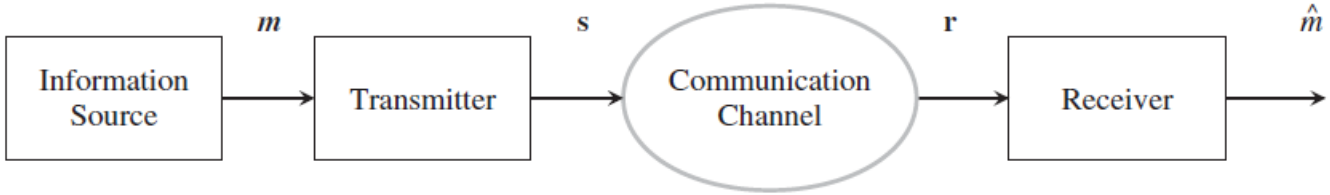

Figure 4.4 Vector equivalent of the system illustrated in Figure 4.1.

4.3 Optimum Detection in a Vector Communication System

4.3.1 Description of a Vector Communication System

Let us initially assume that the complex envelope $r(t)$ of the (filtered) received signal $r_{RF}(t)$ admits a *finite-dimensional vector* representation $\mathbf{r}$ with no loss of useful information (see Section 4.2.1).[1] Then, the system of Figure 4.1 can be replaced by its vector counterpart shown in Figure 4.4, in which finite-dimensional vectors take the place of time-continuous random processes. In particular, each signal appearing in Figure 4.1 is replaced by a vector of proper size N (the problem of selecting a proper value for this parameter is discussed in the following section). In the vector equivalent system the transmitter generates, in response to a message $m \in A_m$, the vector $\mathbf{s} \triangleq [s_0, s_1, \ldots, s_{N-1}]^T$, belonging to the alphabet $A_{\mathbf{s}} = \{\mathbf{s}_i, i = 0, 1, \ldots, N_m - 1\}$, with $\mathbf{s}_i \triangleq [s_{i,0}, s_{i,1}, \ldots, s_{i,N-1}]^T$, according to the correspondence (see (4.1)):

$$\mathbf{s} = \mathbf{s}_i \Leftrightarrow m = m_i. \tag{4.2}$$

The *average energy per message* spent by the transmitter in the transmission of a message is given by:

$$E_m = \sum_{}^{N_m-1} P_i \, |\mathbf{s}_i|^2. \tag{4.3}$$

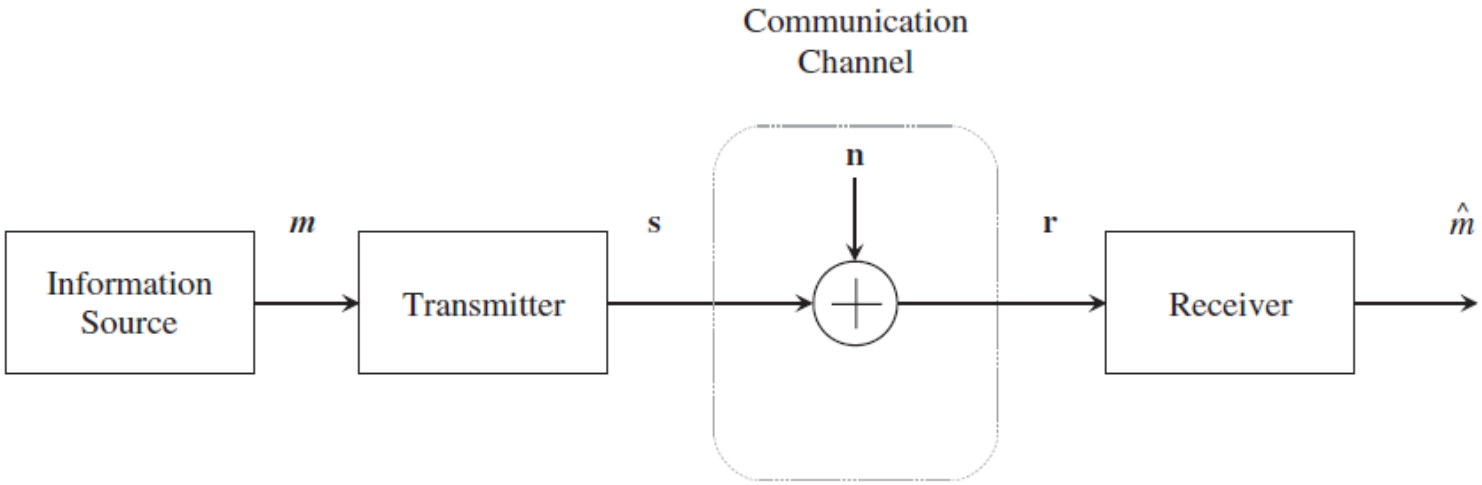

Figure 4.7 Vector communication system characterized by an AGN channel.

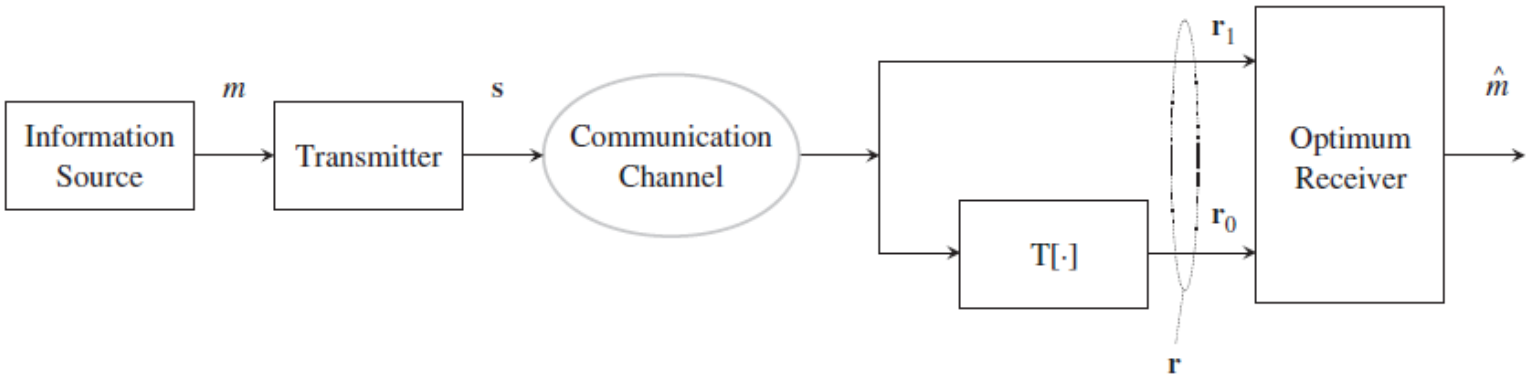

Figure 4.8 Digital communication system useful in proving the *theorem of reversibility*.

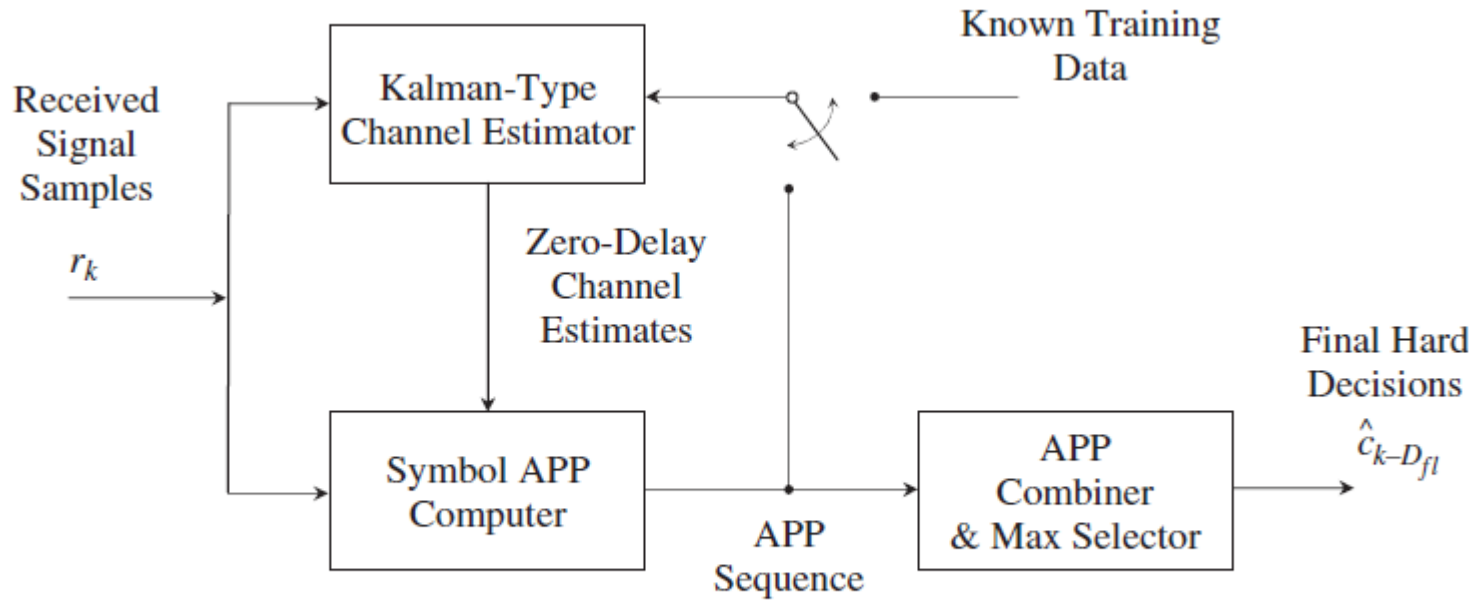

Figure 6.20 Block diagram of an adaptive MAP-FLA with a single channel estimator.

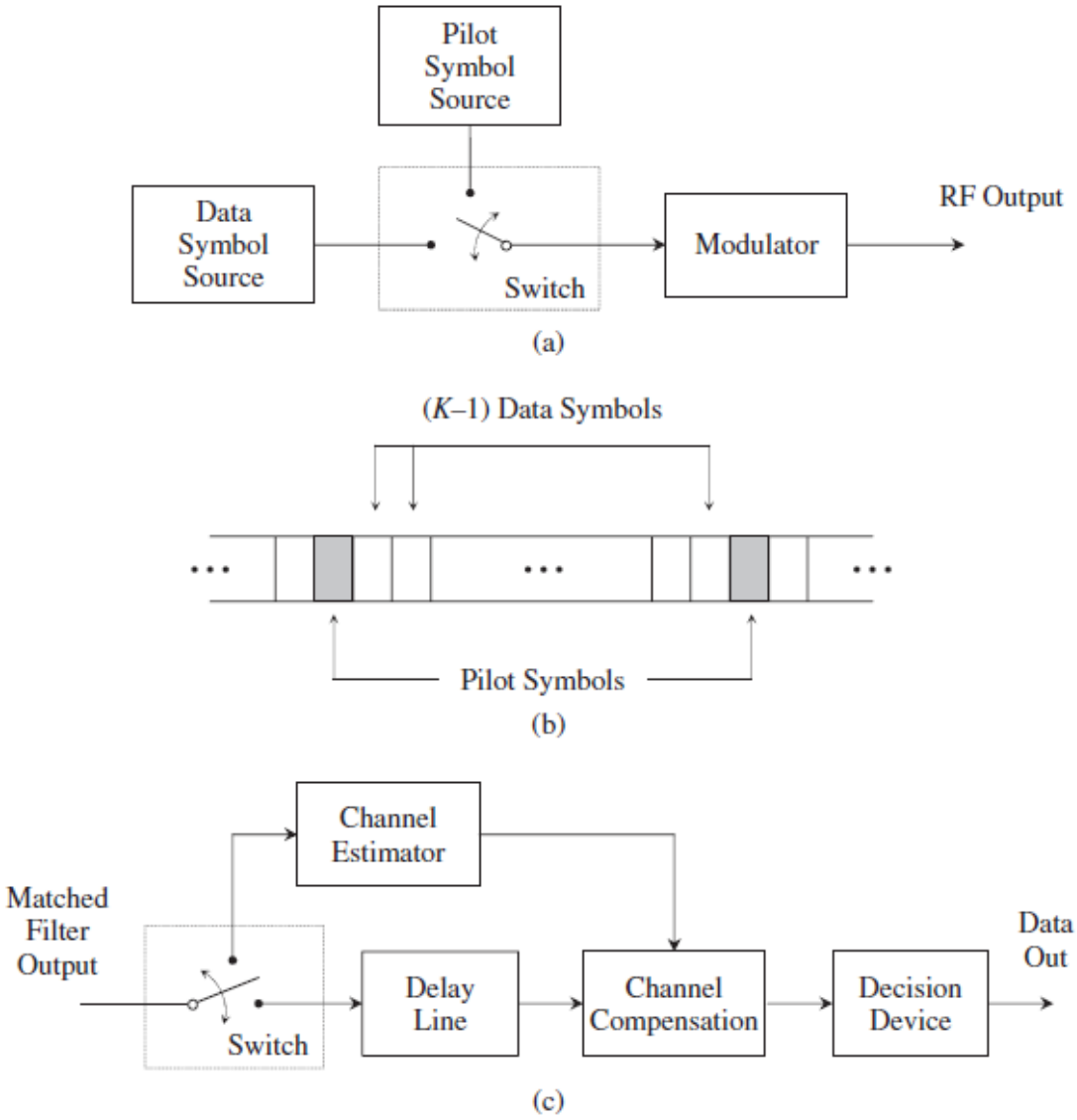

Figure 6.21 Structural block diagram of a PSAM transmitter (a) and receiver (c); location of the pilot symbols in the transmitted symbol sequence (b).

Coding

9.1 Block Codes

9.1.1 Introduction

In this section we focus on *block codes* defined on finite fields.[1] In general, block encoding of information messages can be represented as shown in Figure 9.1. There, an information source generates a sequence of *symbols*, each belonging to GF(q), with $q = p^l$ (p is prime and l is a positive integer). The sequence is partitioned into *blocks*, called *messages*, each of length k. The encoder converts each input message[2]:

$$\mathbf{u} \triangleq [u_0, u_1, \ldots, u_{k-1}], \tag{9.1}$$

in accordance with *one-to-one mapping*, to a vector, called a *codeword*:

$$\mathbf{x} \triangleq [x_0, x_1, \ldots, x_{n-1}], \tag{9.2}$$

[1] An introduction to finite field theory is provided in Appendix E.
[2] In this chapter, unless stated otherwise, row vectors are used.

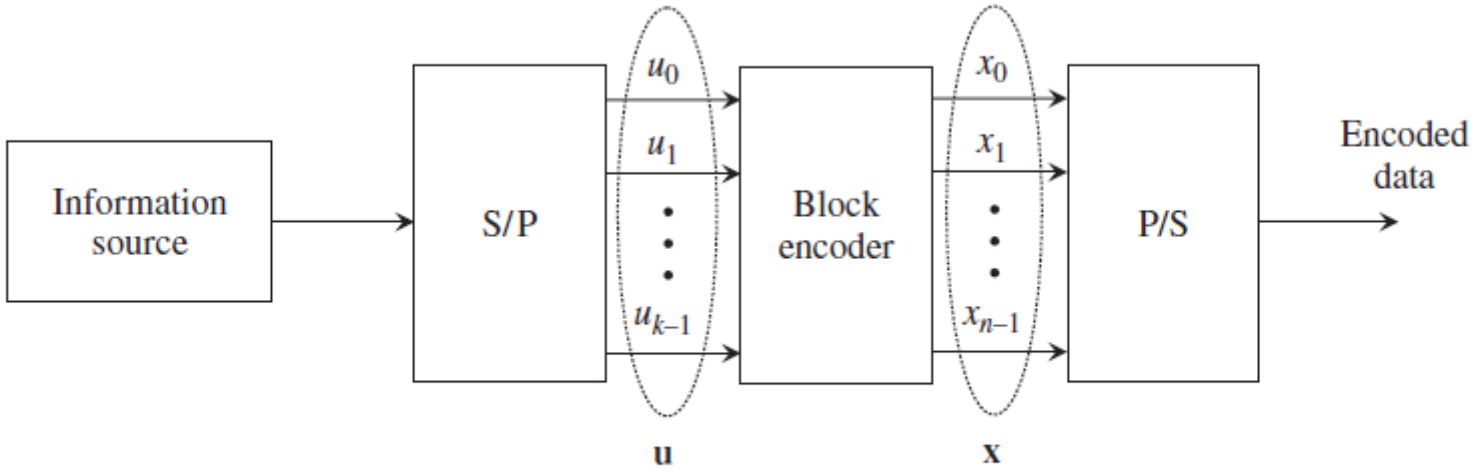

Figure 9.1 Block encoding of a data stream emanating from an arbitrary information source.

Table 9.1 Standard array

$\mathbf{e}_0 = \mathbf{x}_0 = \mathbf{0}_n$	$\mathbf{x}_1$	$\cdots$	$\mathbf{x}_i$	$\cdots$	$\mathbf{x}_{q^k-1}$
$\mathbf{e}_1$	$\mathbf{e}_1 \boxplus \mathbf{x}_1$	$\cdots$	$\mathbf{e}_1 \boxplus \mathbf{x}_i$	$\cdots$	$\mathbf{e}_1 \boxplus \mathbf{x}_{q^k-1}$
$\vdots$	$\vdots$	$\vdots$	$\vdots$	$\vdots$	$\vdots$
$\mathbf{e}_l$	$\mathbf{e}_l \boxplus \mathbf{x}_1$	$\cdots$	$\mathbf{e}_l \boxplus \mathbf{x}_i$	$\cdots$	$\mathbf{e}_l \boxplus \mathbf{x}_{q^k-1}$
$\vdots$	$\vdots$	$\vdots$	$\vdots$	$\vdots$	$\vdots$
$\mathbf{e}_{q^{n-k}-1}$	$\mathbf{e}_{q^{n-k}-1} \boxplus \mathbf{x}_1$	$\cdots$	$\mathbf{e}_{q^{n-k}-1} \boxplus \mathbf{x}_i$	$\cdots$	$\mathbf{e}_{q^{n-k}-1} \boxplus \mathbf{x}_{q^k-1}$

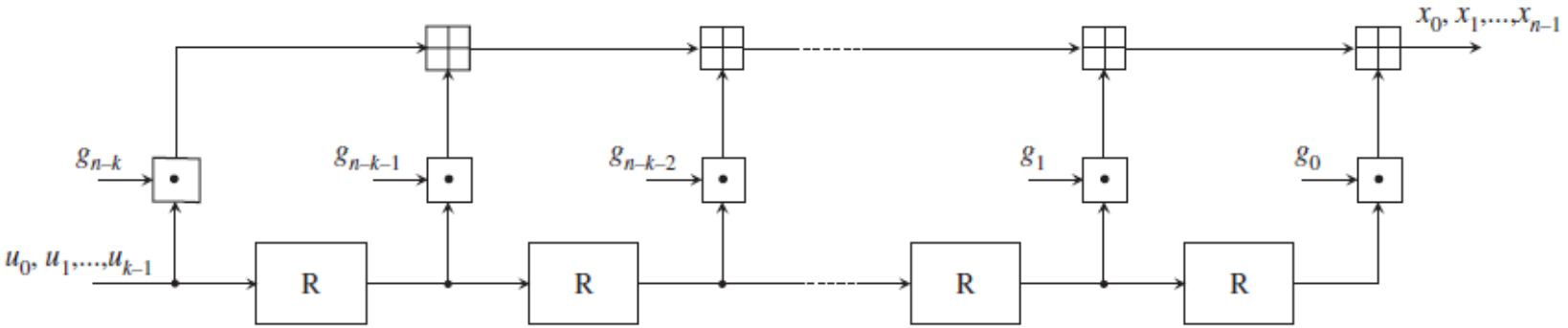

Figure 9.3 Nonsystematic encoder for an (n, k) cyclic code $\mathcal{C}$ over GF(q).

Table 9.2 Cyclotomic cosets and minimal polynomials of GF(16)

Cyclotomic cosets	Minimal polynomials
$C_0 = \{0\}$	D
$C_1 = \{1\}$	$D+1$
$C_2 = \{\alpha, \alpha^2, \alpha^4, \alpha^8\}$	$D^4 + D + 1$
$C_3 = \{\alpha^3, \alpha^6, \alpha^9, \alpha^{12}\}$	$D^4 + D^3 + D^2 + D + 1$
$C_4 = \{\alpha^5, \alpha^{10}\}$	$D^2 + D + 1$
$C_5 = \{\alpha^7, \alpha^{11}, \alpha^{13}, \alpha^{14}\}$	$D^4 + D^3 + 1$

since the cyclotomic coset of β is:

$$\beta = \alpha^3, \quad \beta^2 = \alpha^6, \quad \beta^4 = \alpha^{12}, \quad \beta^8 = \alpha^9, \quad \beta^{16} = \alpha^3 = \beta, \tag{9.69}$$

Table 9.3 Polynomial representation of the elements of GF(16) (where β is a primitive element of GF(4))

Exponential representation	Polynomial representation
0	0
1	1
α	D
α^2	$D+\beta$
α^3	$\beta^2 D+\beta$
α^4	$D+1$
α^5	β
α^6	βD
α^7	$\beta D+\beta^2$
α^8	$D+\beta^2$
α^9	$\beta D+\beta$
α^{10}	β^2
α^{11}	$\beta^2 D$
α^{12}	$\beta^2 D+1$
α^{13}	$\beta D+1$
α^{14}	$\beta^2 D+\beta^2$

$$\Lambda(D) \triangleq \prod_{i=1}^{v} (1 + X_i D) = \sum_{p=0}^{v} \Lambda_p D^p, \tag{9.100}$$

whose roots are the inverses of the error locators $\{X_p\}$. Note that the coefficients $\{\Lambda_p\}$ of $\Lambda(D)$ can be easily expressed in terms of the error locators involved. In fact, from (9.100) it is easily inferred that:

$$\begin{aligned} \Lambda_0 &= 1, \\ \Lambda_1 &= \sum_{i=1}^{v} X_i, \end{aligned}$$

$$\begin{aligned} \Lambda_2 &= \sum_{i<p} X_i X_p, \\ \Lambda_3 &= \sum_{i<p<q} X_i X_p X_q, \\ &\vdots \\ \Lambda_v &= \prod_{i=1}^{v} X_i. \end{aligned} \tag{9.101}$$

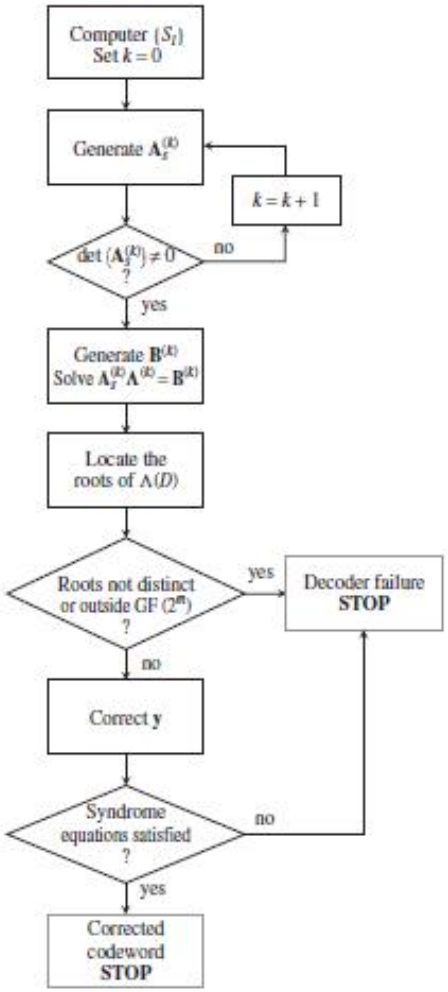

Figure 9.5 Flow diagram of Peterson's direct method for decoding binary BCH codes.

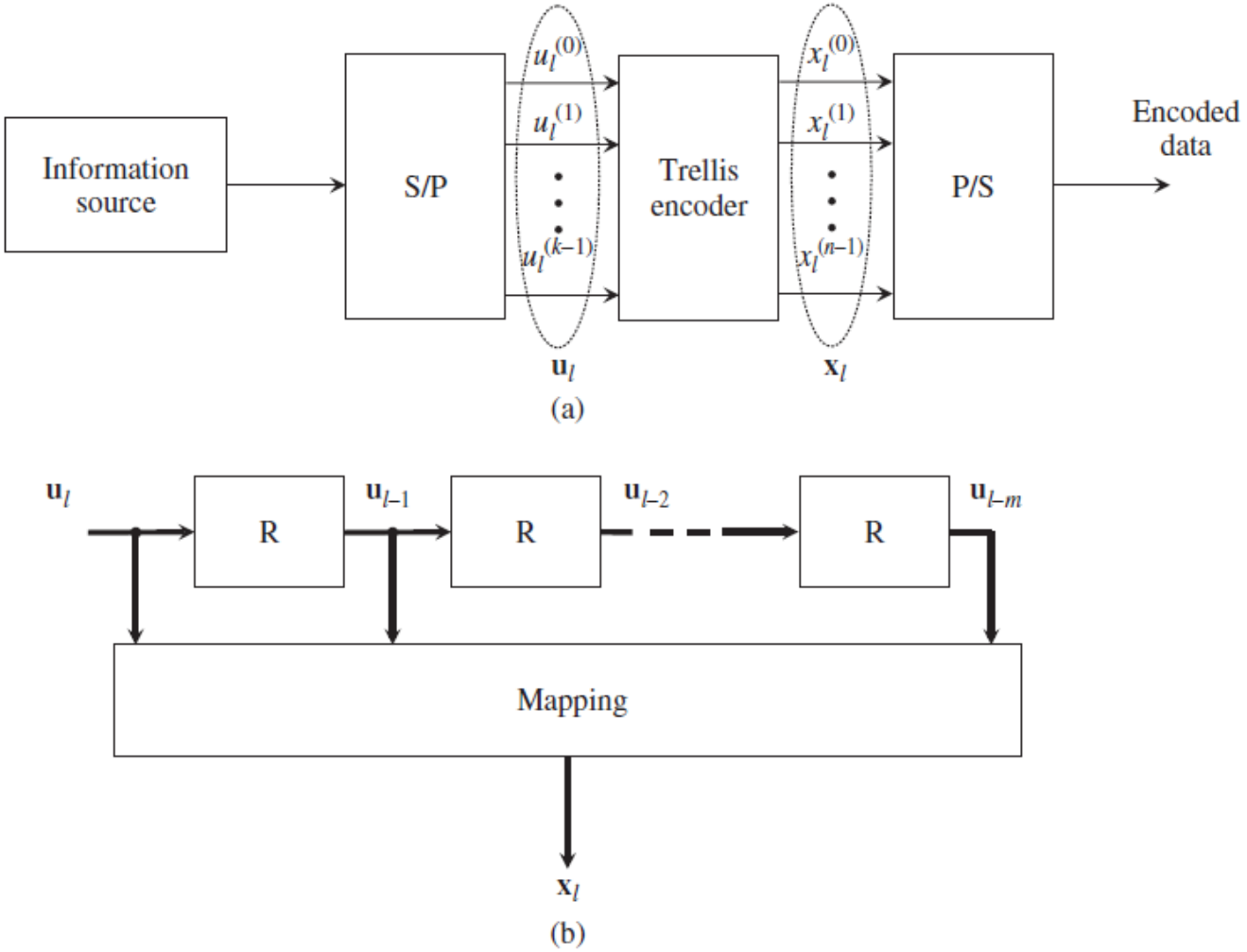

Figure 9.8 Trellis encoder: (a) use in a digital communication system; (b) block diagram.

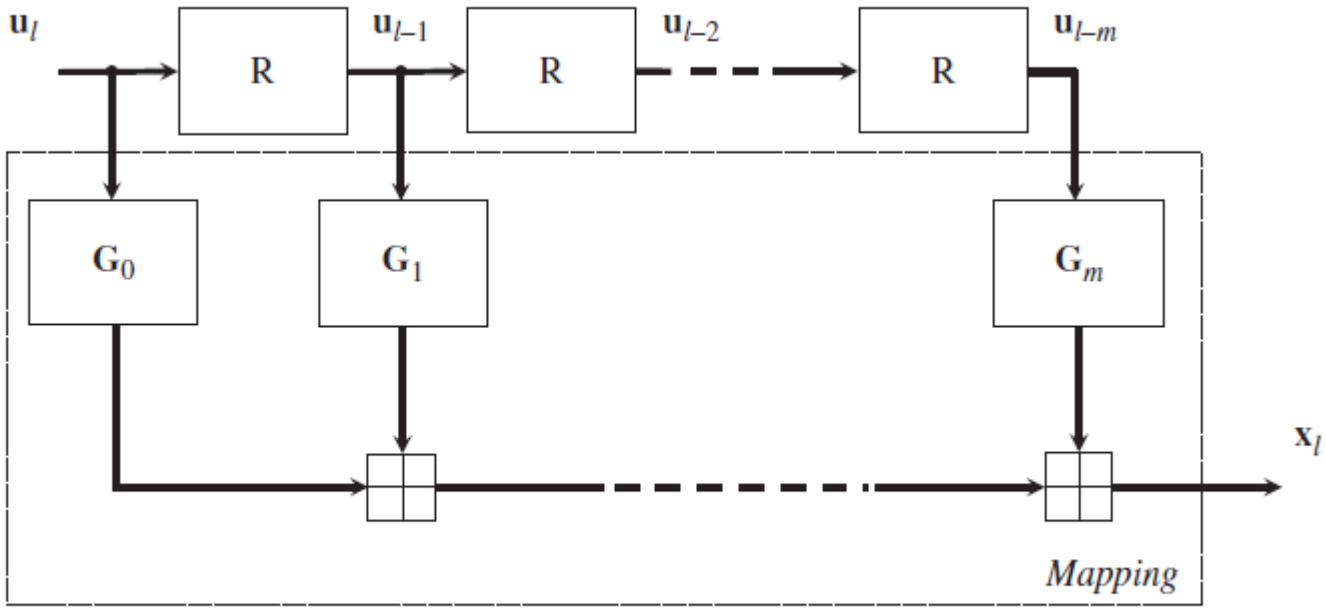

Figure 9.9 Block diagram of a convolutional encoder over GF(q).

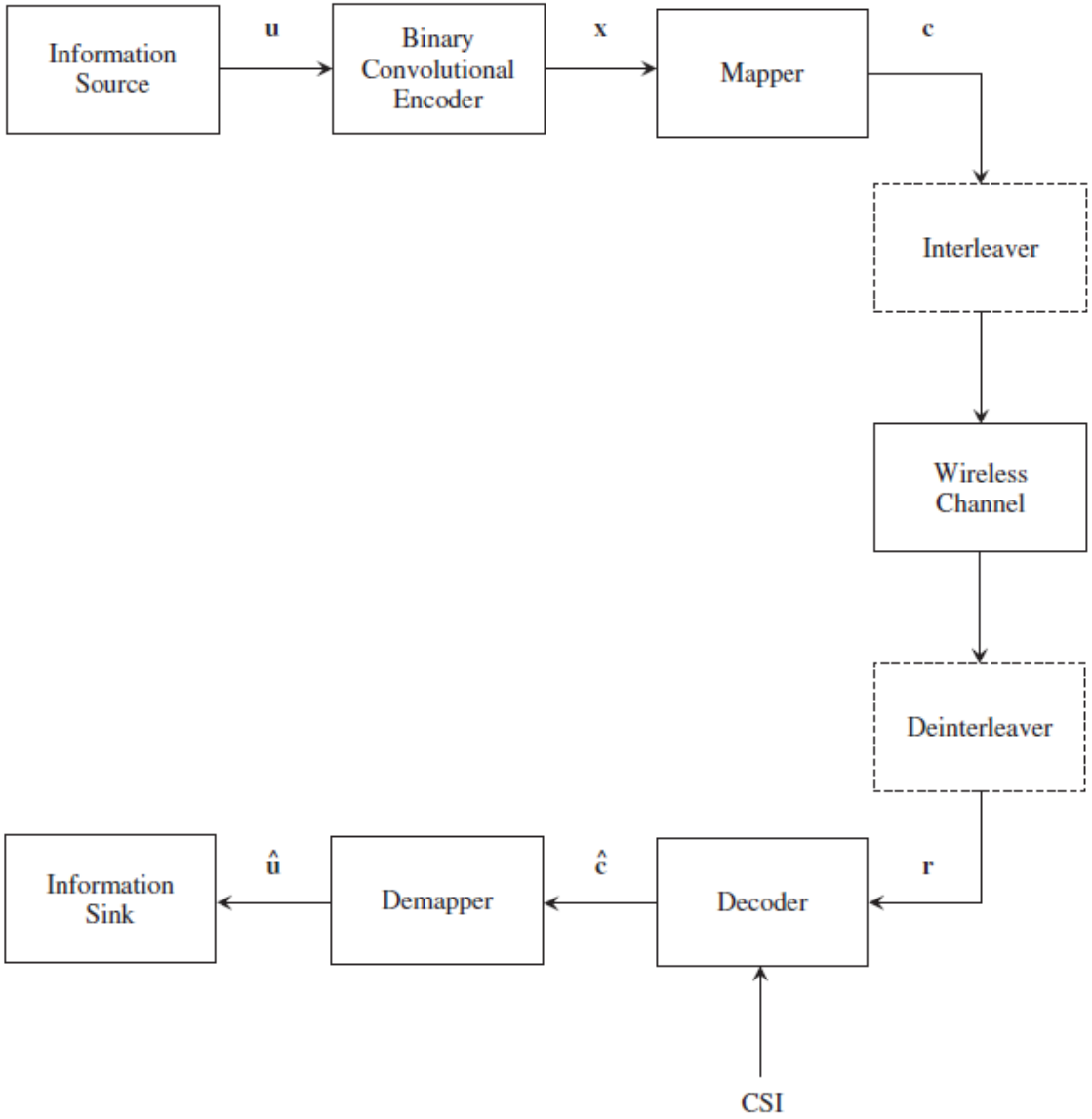

Figure 9.21 Overall block diagram of a wireless communication system employing convolutional encoding.

10.2.1 Parallel Concatenated Coding Schemes

The typical structure of a turbo encoder is illustrated in Figure 10.1. It consists of: two identical binary *recursive systematic convolutional* (RSC) encoders each of rate 1/2 and each with ν memory elements (i.e., 2^{ν} states); and a pseudorandom N-bit interleaver denoted by π in the figure. The first component (RSC) encoder generates the parity sequence $\{c_{1,l}, l = 0, 1, \ldots, N-1\}$ in response to its input sequence $\{u_l, l = 0, 1, \ldots, N-1\}$, consisting of k information bits plus ν termination bits (so that $N = k + \nu$), forcing the encoder to return to its initial state (e.g., the 0 state); this means a *tail-biting* mechanism is used for trellis termination of the given encoder (further details can be found in [37, pp. 183–184] and [1612]) or, equivalently, that a *circular* RSC is used [1605]. The second constituent (RSC) encoder is fed by a permuted version[1] $\{u_{p,l}, l = 0, 1, \ldots, N-1\}$ of $\{u_l\}$ and generates the parity sequence $\{c_{2,l}, l = 0, 1, \ldots, N-1\}$. An optional *puncturing mechanism* can be included in the scheme to modify, when needed, the overall code rate by discarding a part of the parity sequences $\{c_{1,l}\}$ and $\{c_{2,l}\}$ [1613, 1614]. In the absence of puncturing the transmitted codeword $\{x_n\}$ simply consists of the concatenation of the sequences $\{u_l\}$, $\{c_{1,l}\}$ and $\{c_{2,l}\}$, so that the codewords have length $n = 3N$ and the resulting code rate is $R = k/n = (N-\nu)/(3N) \cong 1/3$ for large N.

The following comments are in order concerning the architecture depicted in Figure 10.1, and should be carefully kept in mind when employing it:

1. *Long codewords* should be generated to approach the Shannon limit. In particular, simulation results suggest that the information block length N (and, consequently, the interleaver size) should be chosen to be several thousand bits long. For instance, data blocks of length $N = 65\,536$ and a 256×256 interleaver were adopted in generating the first available results on code performance [1481].
2. *Equal* RSC encoders with a small number of states (e.g., 16 states) are commonly used as constituent codes to achieve excellent performance at moderate BERs [1615, 1616]. Alternatives to this choice include the use of *asymmetric* RSC constituent codes [1617] and block codes (see the next section). The most important parameter in the selection of an RSC code is its *effective free distance* $d_{f,eff}$,

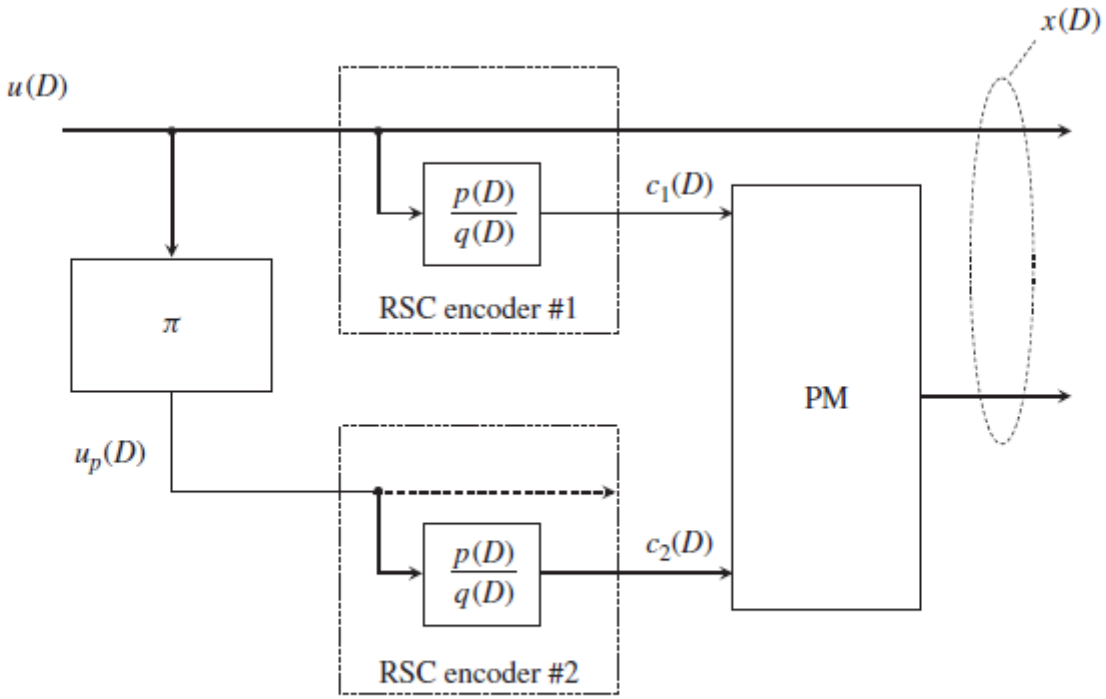

Figure 10.1 Typical PCCC encoder structure.

10.2.2 Serially Concatenated Coding Schemes

Using the same ingredients as PCCCs, namely convolutional encoders and interleavers, SCCCs can easily be developed. The general structure proposed in [1546] for the encoder for an SCCC is illustrated in Figure 10.2(a). In this case, an outer *convolutional encoder* (CE) with rate $R^o = k/p$ feeds a pseudorandom interleaver (π, with a length N that is a multiple of p). Its output is sent an inner CE with rate $R^i = p/n$. This generates an SCCC with rate $R^s = k/n$. RSC codes can be used in this case too, as shown in Figure 10.2(b), describing the serial concatenation of two CEs with $R^i = R^o = 1/2$. The overall code rate $R^s = 1/4$ can be increased by resorting to a proper puncturing mechanism [1614]. Important design guidelines for SCCCs are developed in [1546], where it is shown that: first, it is essential to select an RSC encoder for the inner encoder, since this always yields an *interleaver gain* (defined as the factor by which the bit error probability is decreased with the interleaver length at a given SNR); and second, good outer RSC codes maximize the effective free distance of the inner encoder $d^i_{f,eff}$ (defined, as above, as the minimum weight of the codewords of the inner code generated

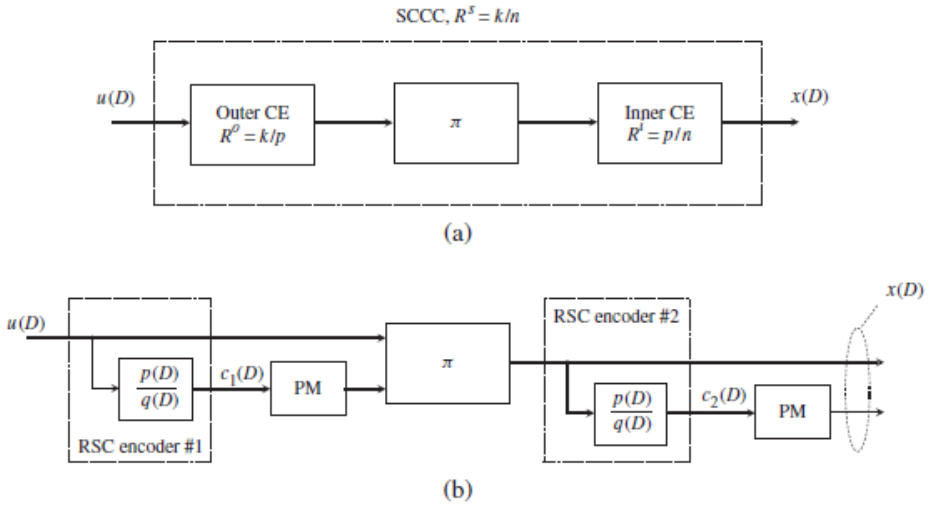

Figure 10.2 (a) General encoder structure of an SCCC scheme and (b) a specific implementation based on the use of two punctured RSCs.

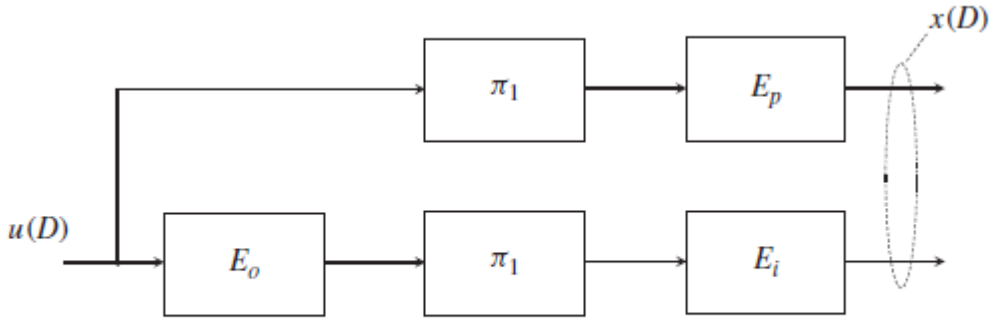

Figure 10.3 General encoder structure of a coding scheme based on *hybrid concatenation*.

10.4.1 *Repeat and Accumulate Codes*

The encoder structure of an RA encoder is illustrated in Figure 10.4. An information block **u** (usually binary) of length N is repeated n times and permuted by an interleaver of length nN. Then the

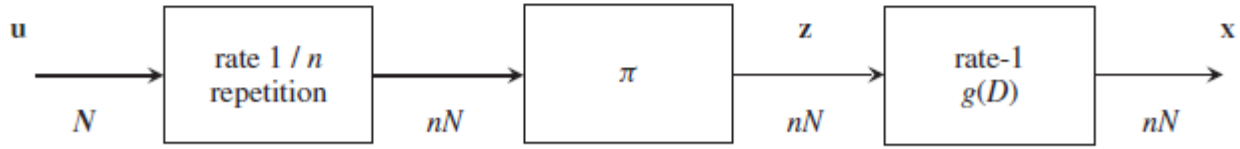

Figure 10.4 Encoder for an (nN, N) RA code. The numbers below the input–output lines indicate the size of the corresponding binary vectors.

11

Signal Space Codes

11.1 Introduction

Hitherto we have mainly focused on binary error-correcting coding. In this chapter we focus on combined coding and modulation. This leads us to look at signal space codes or coded modulations. We will focus on a subset of the available techniques. In particular, we look at the original TCMs, BICMs, *multilevel codes* (MLCs), and *space-time codes* (STCs). In general, the key difference between the design of error control codes and signal space codes is that binary error-correcting codes are typically designed to maximize the minimum Hamming distance between codewords, while signal space codes are generally designed to maximize other distance measures between modulated codewords.

This chapter is organized as follows. The following three sections analyse coded modulation schemes for SIMO communication systems. In particular, trellis coding schemes that exploit expanded signal sets and bit interleaving are described in Sections 11.2 and 11.3, respectively, whereas Section 11.4 is focused on the study of modulation codes based on multilevel coding. The remainder of the chapter investigates space-time coding. In particular, various classes of STCs, including STBCs, OST-BCs, STTCs, layered STCs and unitary STCs, are analysed in Section 11.5. Most of our results refer to SC systems; however, in the last part of Section 11.5, STCs for MIMO OFDM are considered. Finally, some historical information and suggestions for further reading are provided in Section 11.6 and 11.7, respectively.

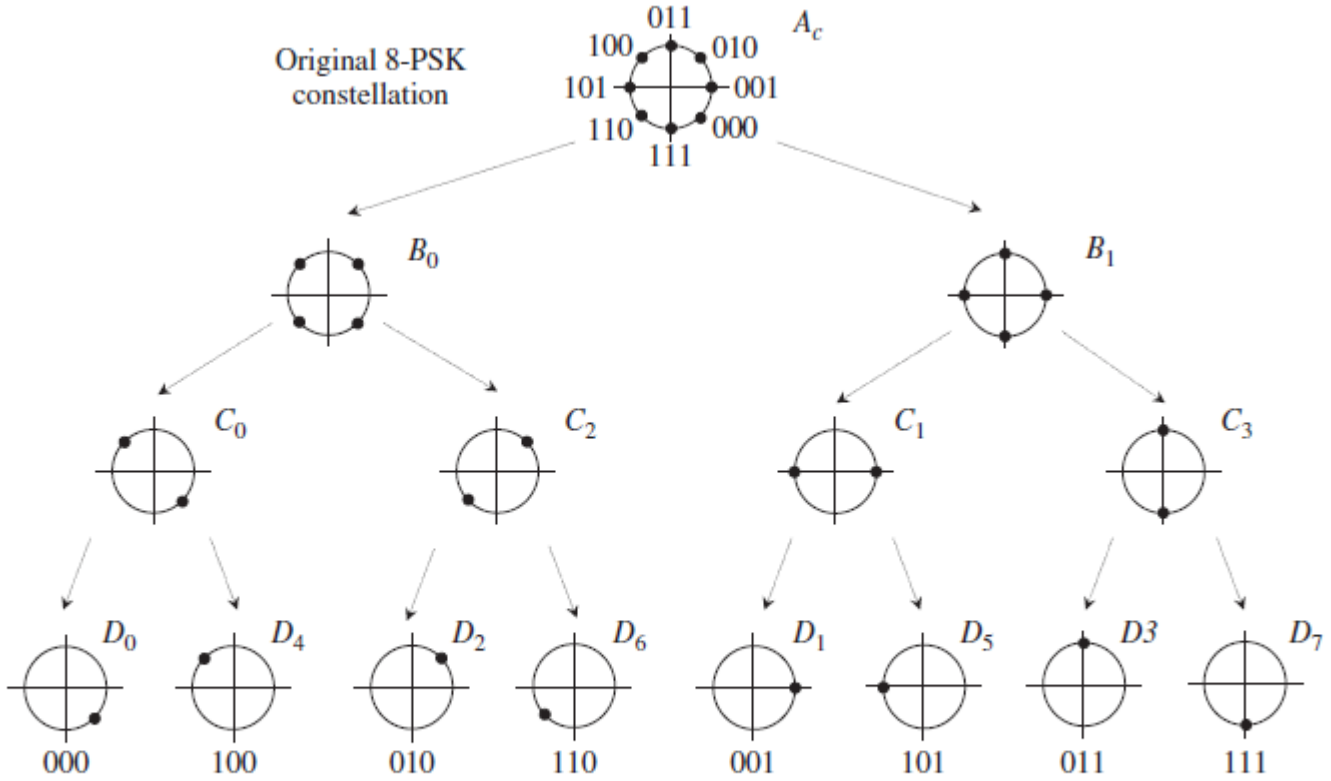

Figure 11.1 Set partitioning of an 8-PSK constellation.

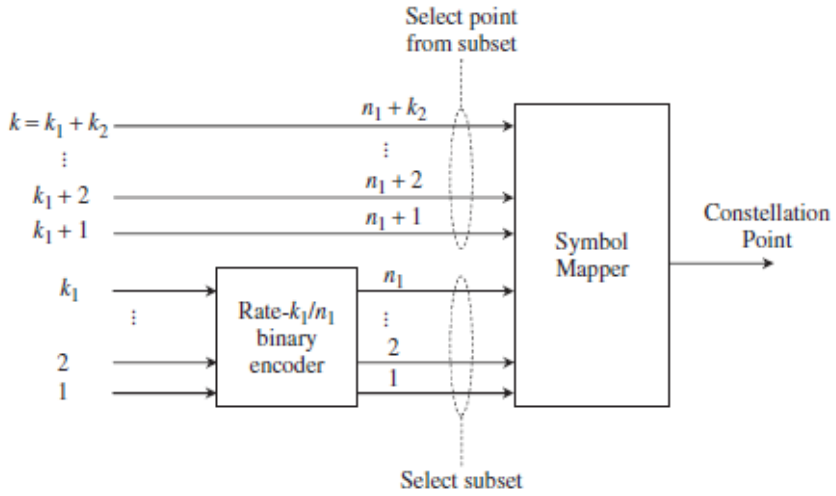

Figure 11.2 Structure of a general TCM encoder for an AWGN channel.

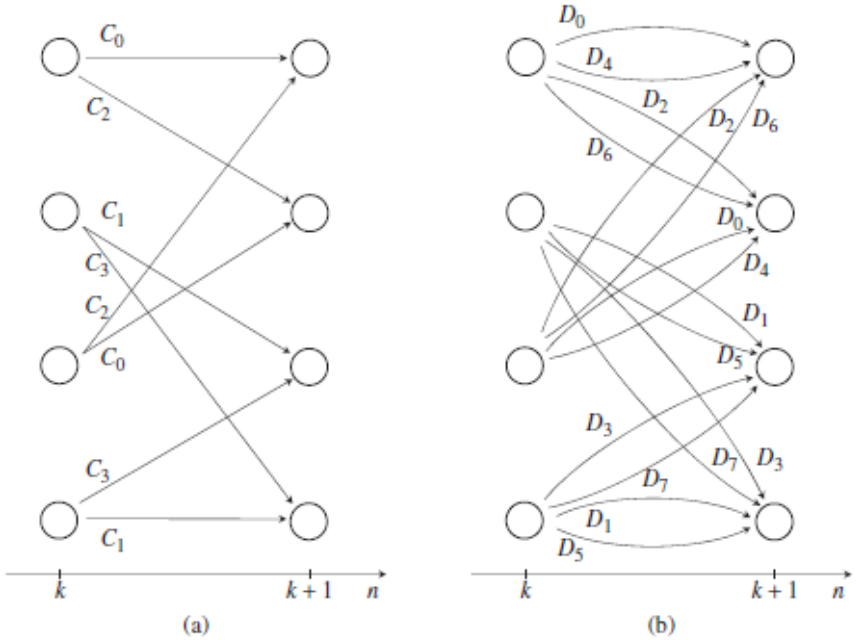

Figure 11.3 Trellis diagrams of the binary encoder and of the overall encoder.

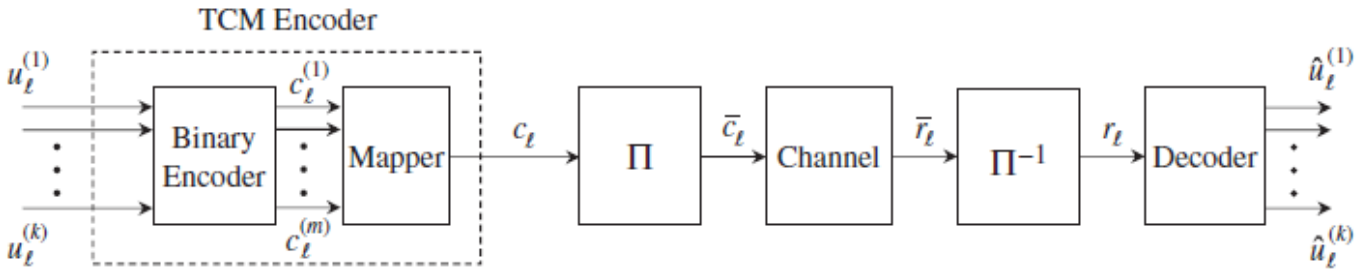

Figure 11.5 Possible transmission scheme adopting a coded modulation over a fading channel.

11.3 Bit-Interleaved Coded Modulation

Beginning with the introduction of TCM, it was generally accepted that coding and modulation must be designed jointly. The same paradigm was adopted on fading channels, although, in this case, the free Euclidean distance no longer plays a predominant role. Instead, as described in the previous sections, the code diversity is the main code parameter to be maximized.

A first deviation from this paradigm is represented by BICM. This technique, originally proposed by E. Zehavi [1464] in 1992, was further developed and analyzed by G. Caire, G. Taricco and E. Biglieri [1854] in 1998. According to this technique, coded modulations with a very good performance over frequency-flat fading channels can be built by using off-the-shelf binary codes that are optimal in the sense of the free Hamming distance, and thus available in standard textbooks.

11.3.1 Code Construction

A system employing BICM is shown in Figure 11.8. The presence at the transmitter of *parallel-to-serial* (P/S) and *serial-to-parallel* (S/P) converters makes clear that the interleaver operates at the bit

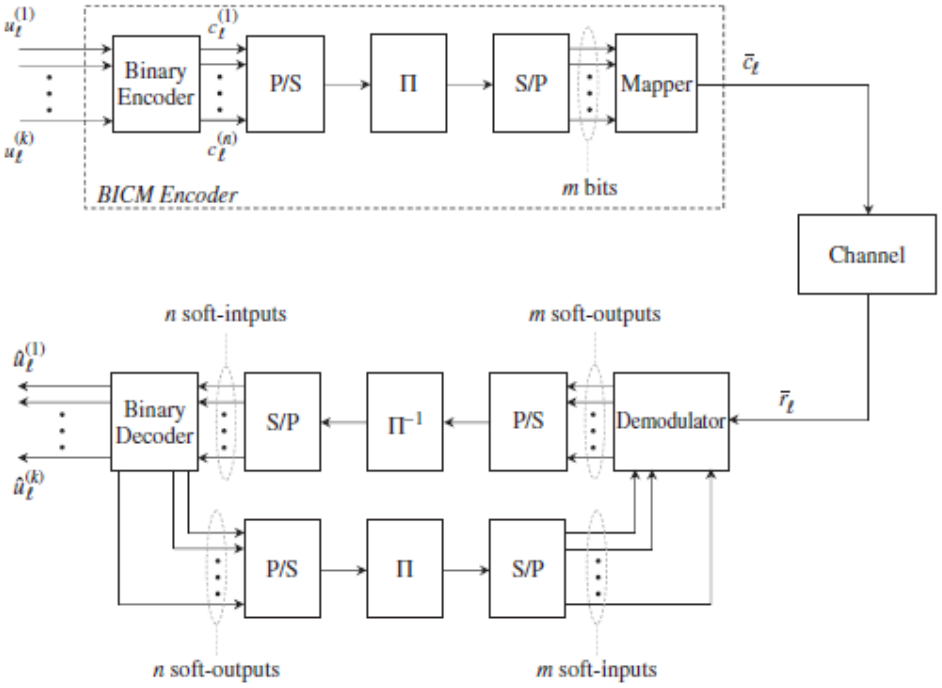

Figure 11.8 Transmission scheme employing BICM.

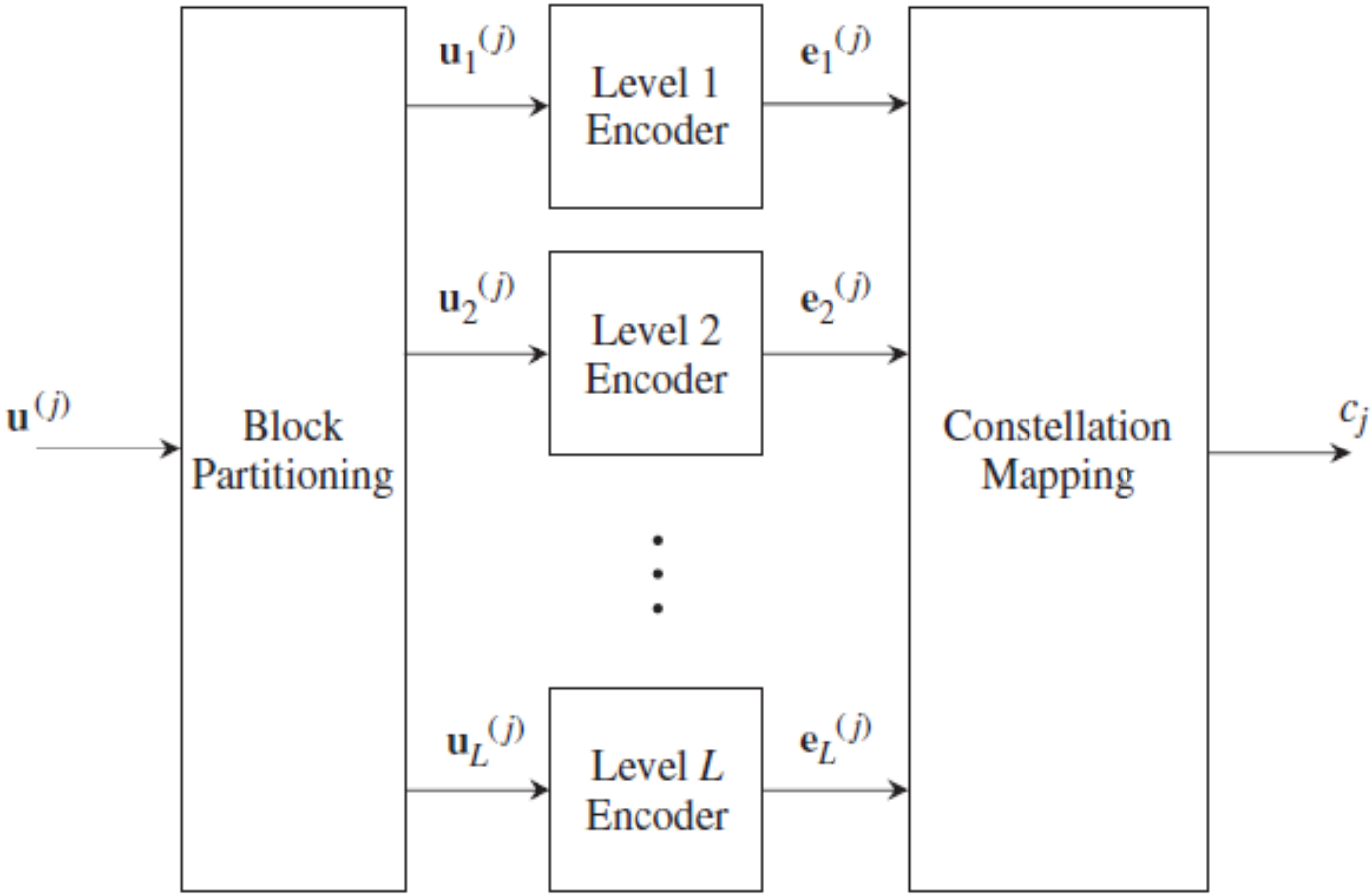

Figure 11.11 L-level encoder.

Multistage Decoder

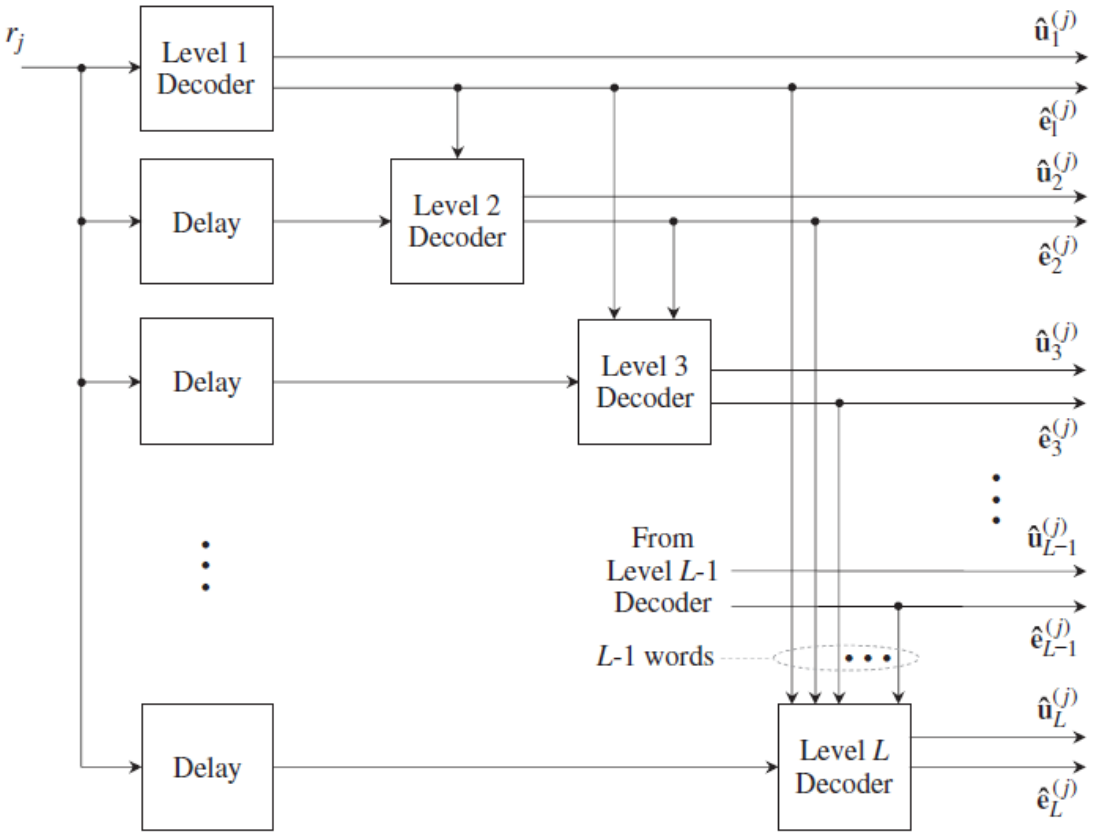

Figure 11.15 L-level MSD, where $\{\hat{\mathbf{u}}_p^{(j)}, p = 1, 2, \ldots, L\}$ are the hard decisions from all levels.

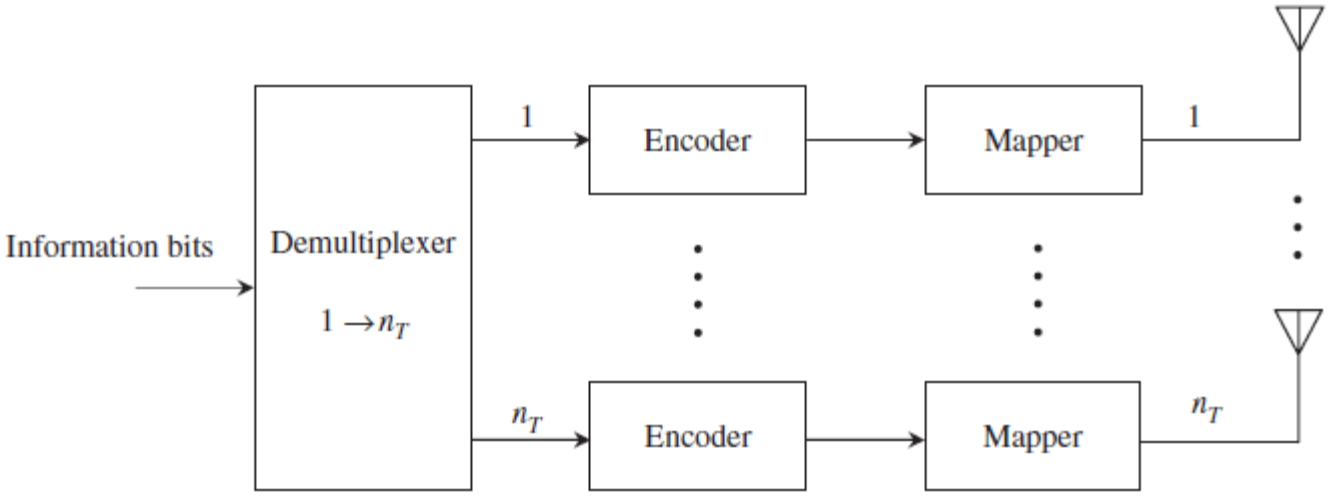

Figure 11.20 H-BLAST encoder.

Threaded ST codes

Threaded STCs (TSTCs) [1905] exhibit superior performance with respect to the scheme in [1904]. In fact, multilayered ST codes have a performance which is 6–9 dB from the outage capacity at 10% frame error rate [1904] whereas the threaded architecture closes the gap to less than 3 dB from the outage capacity with the same frame length, error rate and receiver complexity

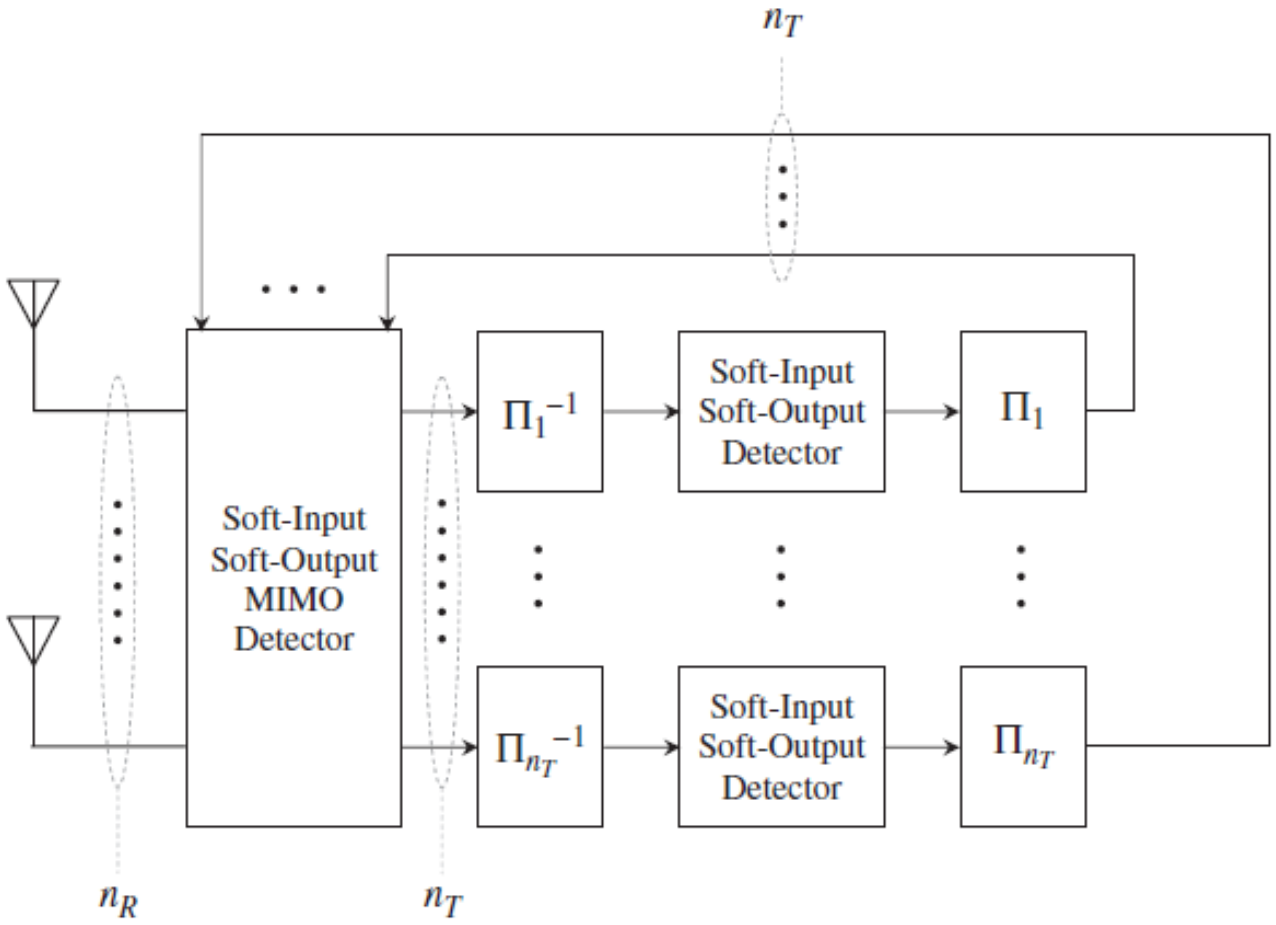

Figure 11.22 TSTC decoder.